LEPL – Batumi Shota Rustaveli State University

Faculty of Exact Science and Education

Department of Physics

Jaba Shainidze

Study of the optical properties of the substance with the software-hardware control of the signal registered by the adaptive semiconductor CCD photo detector

Annotation

Presented for attaining the Academic Degree in Physics

Scientific Advisor: Professor Nugzar Gomidze

Batumi - 2024

Relevance of the topic. A high level of analytical control of the substance and environment is the basis for the success of the production and development of modern technologies. Common methods for analyzing the chemical composition of the environment include numerous optical methods, along with standard chromatographic, gravimetric, and other methods. Selecting an effective and optimal method from numerous optical methods and adapting it to the properties of the investigated substance is currently one of the urgent tasks. Recent studies are devoted to increasing the signal-to-noise ratio and thereby optimizing CCD detectors and are closely related to the thesis topic.

Aim of the research. The aim of the research is to increase the efficiency of photoelectric conversion systems and the efficiency of environmental diagnostics problems detection. Of particular importance is the detection of the light source through the environment, including through the phase screen. The phase screen is an optically dense medium, the modeling of whose characteristics may become the basis for the creation of new types of fast and efficient optical detectors.

Methodology: The research methodology is based on two approaches: 1. Charge-coupled device (CCD) detectors for obtaining high-resolution spectral data, particularly in the ultraviolet (UV) and visible light ranges. CCD detectors are characterized by high quantum efficiency and sensitivity to light, which allows detailed study of spectral lines and of molecular vibrational states. The methodology involves calibrating these detectors to accurately measure the optical density and account for small changes in the spectral data.

2. The analysis is based on the assumption that the electronic transitions in the formation of molecular spectra occur so rapidly that the nuclear positions are essentially unchanged during this process. The intensity of the spectral lines is correlated with the overlap of the vibrational wave functions of the initial and final states, according to the Franck-Condon factor.

The main conclusions of the thesis can be divided into two parts:

1. CCD detectors provided detailed spectral images that revealed distinct patterns of electronic transitions consistent with theoretical predictions. This validated the use of CCD technology in capturing the subtle nuances of molecular spectroscopy, particularly in the UV and visible spectra.

2. The spectral data supported the theoretical framework of the Franck-Condon principle, showing that the most intense spectral lines correspond to transitions between vibrational levels with the greatest overlap of wave functions.

Practical significance of the work. The results of the dissertation research will be important for the development of such studies as:

- **Standardized test procedures:** The use of these procedures among different laboratories and researchers can help ensure consistency in the measurement of optical properties of a substance, such as signal-to-noise ratio or fluorescence spectra.
- **Blind testing:** can be used to reduce the influence of bias on experimental results.
- **Calibration standards:** The use of calibration standards can ensure that measurements made by different researchers and laboratories are comparable.
- **Statistical analysis:** Appropriate statistical analysis can ensure the reliability of the experimental results and confirm the conclusions with the data.
- **Replication studies:** Replication studies can help verify the results of previous studies and increase confidence in the reliability of experimental findings.

Scientific novelty. The novelty of the research lies in the developed methods that increase the overall efficiency of optical-electrical devices in various ways. In particular, a mechanism for increasing the efficiency of the CCD sensor by improving the quantum efficiency is proposed. An evaluation of the use of CCD sensors for some practical applications and ways to improve them are also presented.

The content of the doctoral thesis

In **the introduction of the thesis,** the classification of spectroscopic methods is presented and the main schemes of the photodetector are discussed.

It is emphasized that today spectroscopic methods are classified according to: electromagnetic radiation; according to the interaction of radiation with matter: absorption (absorption spectroscopy), emission (emission spectroscopy), scattering (Raman spectroscopy) and reflection (reflection spectroscopy); according to the objects to be studied: atomic and molecular structure of the object; according to spectrum registration: visual, photographic and photoelectric.

The need to create adaptive photodetectors led to the creation of multi-element semiconductor solid-state detectors, from which we distinguish detectors according to the signal processing method:

- Charge Injection Device (CID)
- Charge-Coupled Device (CCD)

Both detectors are based on silicon, on which photosensitive elements - "pixels" are placed.

CCD sensors are used in a wide range of applications, namely: astrophotography, electron microscopes, and, of interest to us, fluorescence spectroscopy. It is worth noting that these sensors have mainly changed their appearance in consumer digital cameras (CMOS), where sensors with additional metal oxide-semiconductor sensors are used, which are budget-friendly to manufacture. Thus, CCD sensors continue to be the preferred sensors in many scientific and industrial applications.

In the introductory part of the dissertation, the literature related to the work is reviewed. It is noted that the majority of recent works are devoted to the optimization of CCD detectors. The literary sources describing the StellarNet spectrometer, the BlackComet detector, and the Porta LIBS system, which were part of the material-technical base of the dissertation, were analyzed. The relationship between the works performed within the dissertation and the goals and results of the dissertation is reviewed.

Chapter I. Fundamentals and applications of optical-electrical systems.

Main argument: This chapter establishes the physical basis for electronic transitions in molecular orbitals, emphasizing the changes in energy levels that electrons undergo. It proves that despite the differences in the spin-orbital interactions of the molecules, such transitions involve interactions between the spin angular momentum of the electrons and their orbital motion, leading to a splitting of the energy levels.

Research question: How do molecular electronic transitions contribute to understanding the optical properties of substances?

The first chapter of the thesis presents the concept of using CCD photodetectors of semiconductor technology in detecting and recording optical signals. It discusses the importance of signal-to-noise ratio (SNR) estimation in optical density (OD) environments.

§1. Optical density and absorbance are presented. Optical Density (OD) is a measure of light absorption by a substance. It is often used to quantify the concentration of a specific substance in a solution. OD expressed in absorbance units (AU) has been shown to increase in proportion to the increase in light absorption by the sample. OD is an important physical characteristic because it can be used to determine the concentration of a substance in a solution or to estimate the thickness of a thin film. That is why the importance of OD assessment in different fields (chemistry, biology, physics and engineering) is emphasized.

The estimation of OD is related to the measurement of light intensity (I) through the test sample. If the light intensity transmitted in the standard solution (I_0), is known, then its transmission T in the solution with the β attenuation coefficient placed in the cuvette with the L path length determines the OD:

$$T = \frac{I}{I_0} = e^{-\beta L}$$

The light transmission rate decreases exponentially depending on the width of the cuvette:

$$\ln T = \ln\left(\frac{I}{I_0}\right) = \ln\left(e^{-\beta L}\right) = -\beta L = -(\beta_S + \beta_a)L$$

Signal reduction is due to signal scattering (β_S) and absorption (β_a):

$$\beta = \beta_S + \beta_a$$

If the size of the detector is too small compared to the distance traveled by the light (the cuvette's path length), then all the photons that are scattered by the particles of matter in a direct or indirect direction will obviously not reach the detector. In such a case, lnT gives us the effect of superposition of absorption and scattering. Because the absorbed fraction is more prominent than the scattered one, the absorbed fraction is used to quantify the absorbing particles.

The optical density (OD) at a particular wavelength is numerically equal to the absorbance at that frequency:

$$OD = A = -\log_{10} T.$$

It is important to note that the choice of reference sample can affect the calculated OD value. The reference solution should be a solvent or buffer that has the same optical properties as the sample solution.

In the experimental part of the thesis, it was planned to measure the optical density (OD) of the research sample using the StellarNet spectrometer, which uses the BlackComet (190-850 nm) detector. The following works were performed:

- **Spectrometer installation:** Connect the BlackComet detector to the cuvette holder with fiber optic cables, and to the recording device with the USB port. We used StellarNet's SpectraWiz software for signal registration. Installed the software and configured the BlackComet detector license code, specifying the attached parameters.
- **Sample preparation:** Placed the sample in the cuvette and made sure it is properly aligned with the light beam.
- **Capturing the spectra:** Recorded the spectrum of the sample using the spectrometer software.
- **Taking reference spectra:** we placed a control sample - the so-called etalon in the cuvette and we took the spectra. It should be noted that the control sample was the same solvent as the test sample in order to exclude the influence of solvent-induced background absorption.
- **Calculation of OD:** We calculated the OD of the sample.

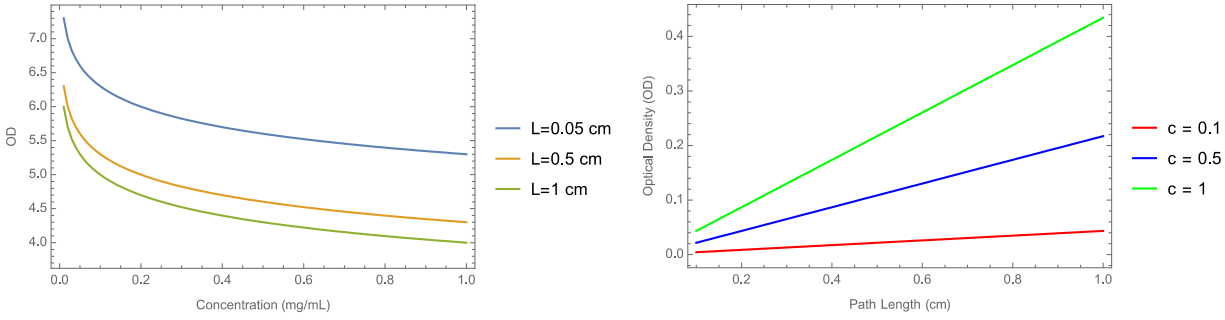

a) b)

Fig.1.1. a) OD vs c, three curves, when the path length is 0.05, 0.5 and 1 cm, $\lambda = 337.1$ nm; b) OD vs L, three lines, when each corresponds to the different concentration value 0.1, 0.5, 1, $\lambda = 337.1$ nm.

The concentration of the solution was chosen so that the absorbance fell within the linear range of the detector, typically 0.2 to 1.0. The concentration affects the accuracy of the measurement, because the absorption of light is affected by factors such as solvent activity, temperature, and the composition of other compounds. BlackComet spectrometers typically use a 1 cm path length cuvette. However, for samples of low concentration or high absorbance, a shorter path length cuvette is suitable to avoid saturation of the detector signal. Conversely, high

concentration or low absorbance samples may require a longer path length cuvette to obtain a measurable signal.

Fig. 1.1. (a) shows the dependence of optical density OD of the sample on the concentration at different lengths of the cuvette path. It has been shown that increasing the path length for a given sample decreases the optical density, which means that the absorption rate increases and vice versa. However, the increase in concentration leads to an exponential decrease in the optical density of the sample. Fig. 1.1. (b) shows the dependence of the optical density on the cuvette path length at different concentrations. This relationship is linear, with a steeper graph of optical density corresponding to a higher concentration.

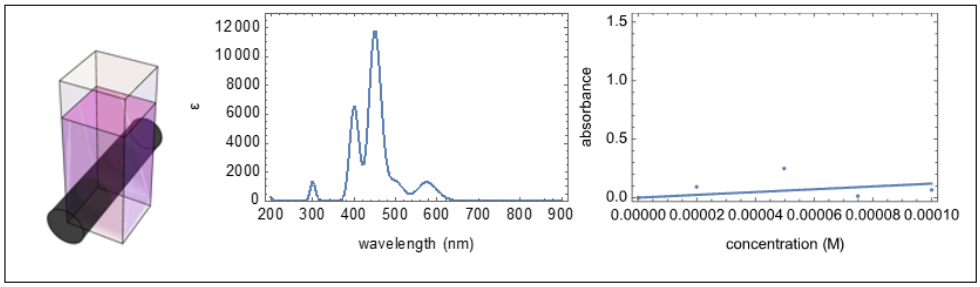

a) wavelength: $\lambda = 300$ nm, molar absorption coefficient: $\varepsilon = 1242.5$ mol^{1} cm^{-1}

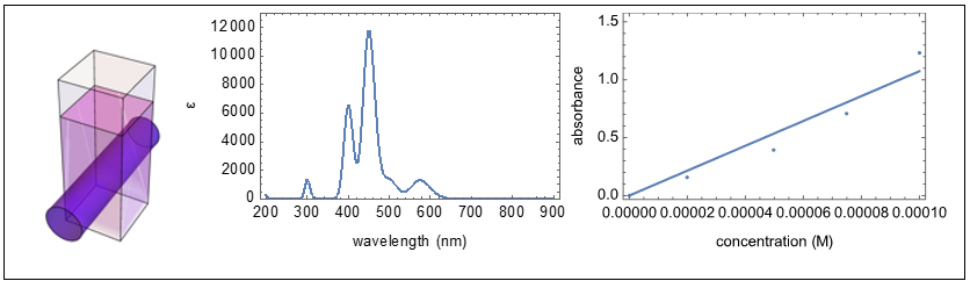

) wavelength: $\lambda = 448$ бð, molar absorption coefficient: $\varepsilon = 11653$ mol^{1} cm^{-1}

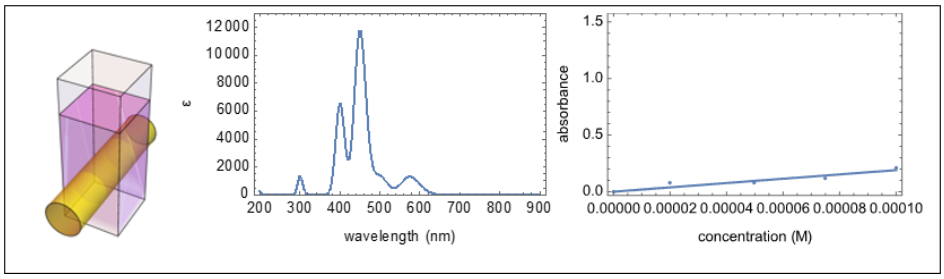

c) wavelength: $\lambda = 574$ nm, molar absorption coefficient: $\varepsilon = 1306.8$ mol^{-1} cm^{-1}

Fig.1.2. The molar absorption coefficient spectrum of the sample. Dependence of absorbance on concentration at different wavelengths, when the concentration of the investigated substances in the sample is $2 \cdot 10^{-6}$ mol

Fig. 1.2 a) shows the dependence of absorption in the ultraviolet range of the spectrum (300 nm) on concentration. Fig. 1.2 b) and c) present corresponding graphs for blue (448 nm) and yellow (574 nm) light.

§2. Ultraviolet and visible light absorption spectra.

This paragraph discusses the absorption spectra of ultraviolet and visible light, when the visible region of the spectrum includes photon energies from 36 to 72 kcal/mol, and in the near-ultraviolet region (up to 200 nm), this energy range increases to 143 kcal/mol. Ultraviolet spectra with wavelengths shorter than 200 nm are difficult to process, so they are rarely used for structural analysis of substances.

The presence of light-absorbing molecular groups - chromophores - in a molecule is best confirmed by UV-visible spectroscopy, but most spectroscopic instruments for wavelengths below 200 nm are practically problematic in terms of detecting isolated chromophores. Fortunately, electron coupling generally causes the absorption maxima to shift to longer wavelengths (for example, in the case of isoprene).

§3. Absorption intensity. It is shown that the molar absorptivity (ε) can be very large for strongly absorbing chromophores (>10000) and very small for weakly absorbing chromophores (from 10 to 100). The magnitude of ε reflects both the size of the chromophore and the probability that light of a given wavelength will be absorbed by the chromophore when light falls on it::

$$\varepsilon = 0.87 \cdot 10^{16}\, PS$$

where P – is the transition probability, it is placed between 0 and 1, S- is the area of the chromophore (in m^2).

§4. Pairing. The analysis of spectral characteristics of different chromophores is discussed in this paragraph. Chromophores are parts of molecules responsible for the ability to absorb light of a specific wavelength, resulting in colored compounds. Concepts such as maximum absorption (λ_{max}), molar extinction (ε) and $\pi \rightarrow \pi^*$ electronic transitions between orbitals are mentioned.

Absorption spectra of pentene and isoprene, bathochromic shifts (shifts to longer wavelengths), hyperchromic shifts (increased absorption intensity) and their relation to double bond conjugation are discussed. This indicates that as the conjugation increases, the wavelength of the absorbed light and the intensity of the absorption increase.

Absorption spectra of various types of chromophores such as ketones, aldehydes and aromatics in the UV and visible range are presented. It is studied how the interaction between orbitals

(HOMO - from the highest energy bonding π-orbital and LUMO - to the lowest energy bonding π-orbital) affects the absorption spectra.

Overall, this paragraph presents a detailed analysis of electronic transitions in molecules and their spectral features, which can be important for understanding the molecular structure and properties of chromophores.

§5. Methods of measuring signal attenuation speed. This section describes methods for measuring signal transmission rates in various types of spectrometers. The working principles of phase and pulse spectrometers, as well as methods of recording fluorescence and phosphorescence spectra are discussed.

In stroboscopic spectrofluorimeters, the beam from the source is divided into two parts. One passes through the test sample and the other passes through the standard sample (etalon), which contains only the solvent. The intensity of the rays is measured by electronic detectors and then compared to determine how much light is absorbed by the sample (Fig. 5.1).

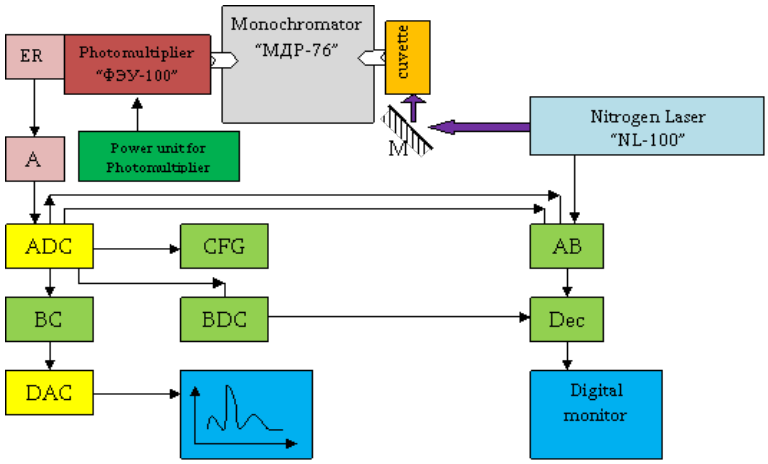

Fig.5.1. Stroboscopic spectrofluorimeter after modernization

M – plane mirror. ADC – Analog to digital converter. DAC - digital-analog converter; ER - emission repeater; A – amplifier; BC - binary counter; BDC - Binary Decadal Counter; Dec – decoder; AB – automatic block; CFG – Calibrated frequency generator.

It should be noted that pulsed spectrometers are simple tools for e.g. fluorescence lifetime measurements. The sample is illuminated by a pulsed light source. The pulse duration is shorter

than the fluorescence lifetime. Fluorescence emission is recorded on an oscilloscope or through electronics consisting of analog-to-digital converters on a personal computer.

The pulse source and the photomultiplier switch at a frequency of several thousand repeats per second, but with a certain delay. Fluorescence curves are recorded by measuring the delay time between excitation and recording. The amplified signal received from the photomultiplier is recorded as a function of delay time through the detector. The pulsed light source used during this method should have a pulse duration shorter than the fluorescence signal attenuation time, so it is convenient to use pulsed hydrogen lamps as a light source. In the second method, the photomultiplier works in pulse mode and has high sensitivity.

In phase fluorometers fluorescence is excited by a cone of light modulated at a high frequency. The fluorescence phase, i.e. the degree of modulation, is compared to the phase of the excitation light. In the case of fluorescence decaying exponentially with time, the phase shift ψ between the fluorescence radiation and the excitation light phases is determined by the expression: $\omega\tau = tg\psi$, where τ - is the fluorescence lifetime. The signal from the source and the fluorescent signal excited on the sample meet the CCD-detector, which registers the phase shift between these signals. The degree of modulation in the excitation light cone (m_s) and the degree of modulation of the fluorescence signal (m_f) are related to the phase shift ψ in the ratio: $\frac{m_f}{m_s} = cos\psi$.

In principle, one of the main drawbacks of the phase fluorometer lies in the difficulty of interpreting the results that arise from non-exponential decay of fluorescence, although Birks, Dyson and Munro used this method for non-exponential decay of fluorescence as well. In the first phase fluorometers, polarized excitation light and the Kerr effect were used to modulate the light cone. In this case, a high-frequency field acts on the liquid or crystal with the electron-optical effect.

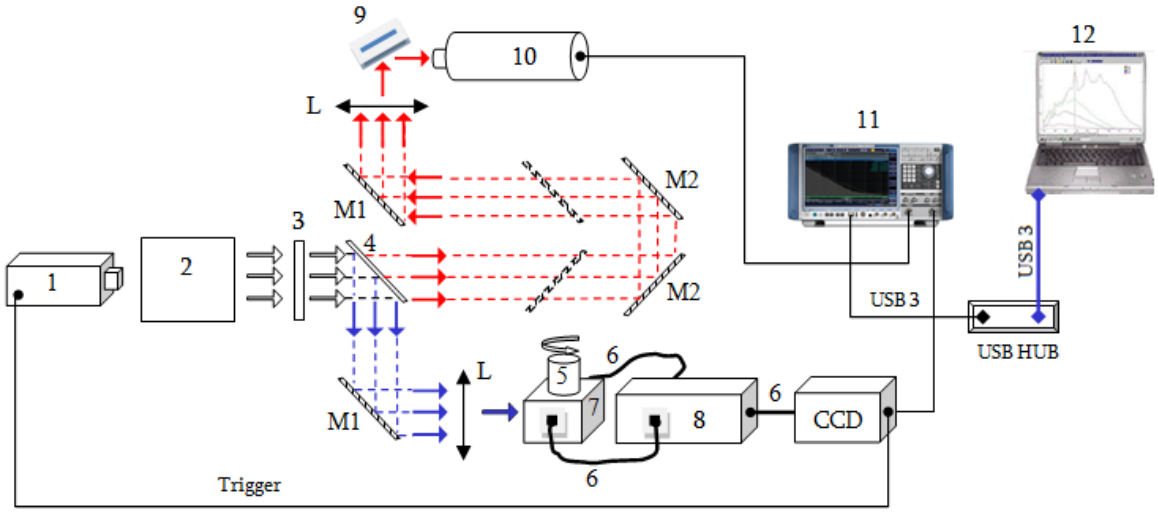

Fig. 5.2. Schematic diagram of a phase fluorimeter. 1- light source, 2 – optical modulator; 3- optical filter, 4- Semi-transparent plate (light divider); 5 - A cuvette with a sample that can be rotated at a constant speed; 6 - Fiber optic light carriers; 7 - Cuvette holder; 8 - correlator; 9 – scattering plate; 10 – photomultiplier; 11 - phase meter; 12 - computer; M1 - Fixed mirror; M2 - moving mirror; L - Converging lens; CCD – Detector.

Thus, the phase fluorometer allows to determine the duration of the glow of the received signal through the phase screen of the support signal with known modulation. Knowledge of the polarization of the source is important in determining the regularities (viscosity, temperature, structure) of the phase screen measurement.

With our proposed method, the fluorescence lifetime can be determined indirectly. This method was first proposed by **Eisenthal**, who described an indirect method of measuring fluorescence emission (10^{-11} s).

It is highlighted how different solvents (water, ethanol, hexane and cyclohexane) affect the measurements. It is explained that solvents with double or triple bonds or heavy atoms (such as S, Br and I) are not used due to high light absorption, which can distort the spectral image.

§6. Characteristics of the CCD sensor of the BlackCommet detector. The paragraph describes the sensor characteristics of the CCD detector used in the BlackComet Spectrometer. A CCD (charge-coupled device) consists of light-sensitive pixels that, when irradiated with photons, generate an electrical charge that is stored in these pixels and then read and converted into a digital signal. CCD detectors are light sensitive and can detect very low levels of light intensity with high accuracy and have a wide dynamic range.

The following main characteristics of CCD sensors are discussed:

- **Quantum Efficiency (QE):** This is the ability of the sensor to convert photons into electrons. QE is usually expressed as a percentage. It depends on the wavelength of the light, the thickness of the active layer and the type of material used in the detector.
- **Dark Current:** It is the flow of electrons that occurs in the absence of light. Dark current is caused by thermal fluctuations of electrons. Obviously, as the temperature increases, the dark current becomes more important. Dark current can result in a higher level of thermal noise (hereafter simply noise) and a lower SNR (Signal-to-Noise Ratio) value.
- **Read Noise:** This is the noise produced when electrons are read from the CCD sensor. Readout noise depends on the electronics used for the readout and can be reduced by cooling the sensor.
- **Full Hole Capacity:** This is the maximum number of electrons that can be stored in a pixel before saturation. The full bandwidth of the holes provides better dynamic range and reduces the possibility of saturation.
- **Pixel Size:** This is the physical size of the individual pixels in the CCD sensor array. Smaller pixel sizes allow higher spatial resolution, but at the same time, can lead to higher noise levels.
- **Linearity:** This is a measure of how well the detector responds to the number of photons detected. The response of a perfectly linear detector is directly proportional to the number of photons detected. Non-linearity can cause image distortion and affect the accuracy of measurements.

It is discussed how these parameters can affect the performance of the CCD detector in spectrometers and how they can affect the optical density (OD) of the sample.

The fraction of photons that hit the detector produces an electron-hole pair. The number of electrons generated per unit of time is estimated by the current produced by the detector (I), the optical power of the light falling on the detector (P) and the active area of the detector (S):

$$I = QE \cdot P \cdot S .$$

The method of estimating the amplification factor of the output signal ($G = \frac{N_e}{N_{ph}}, N_e$ is the number of collected electrons and the number of photons incident (collision) on N_{ph} pixels) and its dependence on signal-to-noise ratio (SNR) is discussed.

$$SNR = \frac{N_e \cdot G}{\sqrt{ND + NR + NF + N_e \cdot G}},$$

where: ND – is the dark noise, NR – reading noise and NF – is fluctuating (statistical) noise.

Formulas for calculating SNR are presented and factors that can affect the accuracy of OD measurements are discussed (Fig. 6.1), including exposure time and the intensity of the light source used to illuminate the sample:

$$OD = -\log_{10}\left(\frac{Signal + Noise}{QE \cdot Intensity \cdot Path\ length}\right).$$

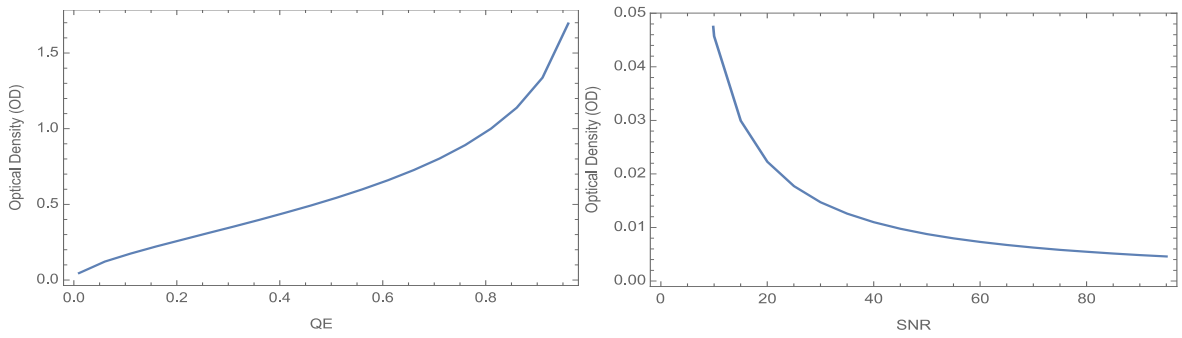

a) b)

Fig.6.1. a) The dependence of OD on QE, b) Dependence of OD on SNR

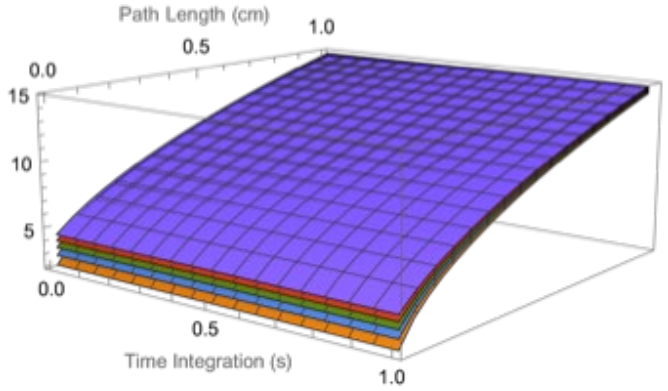

6.2. SNR three-dimensional dependence on beam path length and detector integration time when the concentration is: $c = 0.01$ mol/L, and molar absorption coefficient $\varepsilon = 20000$ L/(mol·cm)

The experimental part of our study was performed on the StellarNet detector BlackComet. BlackComet spectrometers are equipped with high-performance CCD sensors, which are characterized by excellent sensitivity, they have a low noise level in a wide range of wavelengths (Fig. 6.2). These detectors feature a thermoelectric cooling system to reduce noise levels and increase stability. This is why these detectors are ideal for applications such as absorption/transmission spectroscopy, fluorescence spectroscopy, and Raman spectroscopy.

§7. Methods for improving the quantum efficiency (QE) of the CCD sensor. This section describes various methods and strategies for improving the quantum efficiency (QE) of CCD sensors used in spectroscopy. Factors affecting QE, such as sensor material, design, inner layers, ability to reduce surface recombination, etc., are discussed.

Overall, there are many possible ways for future research to improve the performance of CCD sensors used in spectroscopy, and this can have a significant impact on the sensitivity, stability, and accuracy of spectral measurements.

From the listed problems, we should especially mention the researches carried out to improve the quantum efficiency (QE) of CCD sensors. This circumstance will give us a higher QE and can lead to better sensitivity and signal-to-noise ratio.

One of the techniques to optimize the characteristics of the CCD sensor of the BlackCommet detector is to control the hardware capabilities in software. From this point of view, the following studies should be highlighted:

- Image processing algorithms: Implementing efficient image processing algorithms can help reduce noise and improve the detector's signal-to-noise ratio. This may include techniques such as background subtraction, flat-field correction, or deconvolution.
- Timing and synchronization: The timing and synchronization of the detector can affect its performance. Optimizing these parameters will help improve the stability and accuracy of measurements. This may include techniques such as precision trigger implementation, integration time optimization, or readout noise minimization.
- Data collection and storage: Efficient data collection and storage can help improve the speed and accuracy of measurements. This may include techniques such as optimizing data transfer rates, implementing real-time data compression, or implementing a fast data storage system.

Practical steps are also described, and the code in Mathematica programming language is presented, which illustrates the process of image processing from the CCD detector. Steps such as background subtraction, field plane correction, and more are described.

Chapter II. Theoretical analysis of electronic transitions and vibrational processes - Franck-Condon principle in spectroscopic applications

Hypothesis: The basic hypothesis we rely on is the Franck-Condon principle, which provides a theoretical framework for understanding vertical electronic transitions between different vibrational levels within molecules. This principle is crucial for analyzing the intensity and position of spectral lines, thus allowing the estimation of vibrational states of electronic transitions.

Methodology: The research methodology relies on CCD technology to visualize these transitions in the ultraviolet and visible regions of the spectrum. The discussion in this chapter covers the evaluation of the quantum efficiency of CCD detectors and the high-precision measurement of optical density.

§ 2.1. Study of the optical properties of matter at the molecular level with a CCD detector. Franck-Condon principle. The first paragraph of the second chapter of the dissertation is devoted to the study of the optical properties of substances at the molecular level using CCD detectors. It discusses the Franck-Condon principle and its role in visualizing spectral information. This principle is related to electronic transitions in molecules, especially in the ultraviolet and visible spectral regions. It is noted that vibrational changes in molecules are accompanied by electronic transitions.

It is described how CCD devices convert incident photons into an electrical signal that can be used to determine the details of the electronic and vibrational states of molecules.

Analysis of the intensity and position of the spectral lines provides information about the vibrational state and their compliance with the Franck-Condon principle.

The dipole transition matrix element is discussed:

$$\langle e, v|\vec{m}|e', v'\rangle = \int \Psi^*_{ev}\, \vec{m} \Psi_{e'v'} d\vec{r} d\vec{R}.$$

which includes the wave functions describing the oscillatory motion of nuclei: $\Psi_{ev} = \psi_e(\vec{r}, R)\psi_v(\vec{R})$, quantum numbers of the electronic state (e) and - oscillating state (v). It is shown that when $\psi_v(\vec{R})$ is a rapidly oscillating function, and ψ_e changes slowly compared to $\psi_v(\vec{R})$ when R changes, as a special case, we can obtain an image for the matrix element of the dipole transition, which will be related only to the electronic state of the molecule:

$$\langle e|\vec{m}|e'\rangle = \int \psi_e^* \, \vec{m} \psi_{e'} d\vec{r}.$$

In cases where the vibrational quantum numbers are large enough ($v, v' \gg 1$), the motion of molecular nuclei can be considered semi-classical. Nuclei spend most of their time near the equilibrium point and have zero momentum.

It is considered that when the Franck-Condon factor is large, accordingly, the probability of electronic transition is high for such initial and final states, between which it is possible to transition without changing the coordinates of nuclei and moments of momentum.

§ 2.2. Computation of the n-dimensional Franck-Condon overlap integral. The mentioned paragraph presents the quantum-mechanical foundations of the Franck-Condon effect. Discusses and uses it in the calculation of overlap integrals, which play a key role in molecular spectroscopy and describe the probability of overlapping energy bands.

First, the importance of Franck-Condon for the study of optical properties of substances is explained, then a 2008 study (J.L. Chang, 2008) is cited, in which a simplified method for calculating multidimensional Franck-Condon integrals based on the harmonic oscillator wave function and taking into account the Dushinsky effect is proposed. Then the n-dimensional Franck-Condon integral is calculated:

$$\begin{aligned}\langle v_1 v_2 \dots v_n | v_1' v_2' \dots v_n' \rangle = \\ = N \\ \times \int_{-\infty}^{\infty} \int_{-\infty}^{\infty} \dots \int_{-\infty}^{\infty} \prod_{i=1}^{n} \left[exp\left(-\frac{1}{2}\alpha_i' {Q_i'}^2\right) \times H_{v_i'}\left(\sqrt{\alpha_i'} Q_i'\right)\right] \\ \times \prod_{i=1}^{n} \left[exp\left(-\frac{1}{2}\alpha_i {Q_i}^2\right) \times H_{v_i}\left(\sqrt{\alpha_i} Q_i\right)\right] dQ_1 dQ_2 \dots dQ_n.\end{aligned}$$

where, $\langle v_1 v_2 \dots v_n|$ - the column vector corresponds to the initial vibrational state of the molecule, $|v_1' v_2' \dots v_n'\rangle$ - corresponds to the final vibrational state of the molecule, while:

$$N = \frac{1}{\pi^{n/2}} \left(\frac{\sqrt{\prod_{i=1}^{n} (\alpha_i \alpha_i')}}{2 \sum_{i=1}^{n} (v_1 + v_i') \prod_{i=1}^{n} (v_i! \, v_i'!)} \right)^{1/2}$$

is the normalization coefficient. The n-dimensional Franck-Condon overlap integral was verified based on the simulation of the vibrational peak spectrum of SeO_2^-.

In the harmonic approximation for wavefunctions of states, each vibrational state is represented by the product of a normalization factor and a Hermitian polynomial multiplied by an exponential factor. It describes a matrix element between two vibrational states. This element relates the initial and final vibrational states of the molecule and is used to calculate the probability of transitions between these states in emission and absorption processes.

§ 2.3. Modeling of electronic transitions in a diatomic molecule. The third paragraph of the second chapter discusses the modeling of electronic transitions in diatomic molecules, when the interaction between particles is described by the Morse potential energy function. The Morse equation is used to describe the potential energy as a function of the distance between atoms in a molecule:

$$V(\omega, d, \rho, r) = D\left(1 - e^{-3\sqrt{\omega D}(r-\rho)}\right)^2$$

where: $\omega = \omega_0/\omega_1$ - is the ratio of the frequencies of the excited and ground states, $D = D_1/D_0$ - represents the ratio of dissociation energies in excited (D_1) and ground (D_0) states, $\rho = R_1/R_0$ - is the ratio of distances between nuclei at equilibrium, R_1 - corresponds to the equilibrium excited state, and R_0 is the equilibrium basic state. ρ - represents the equilibrium bond length, that is, the distance between particles when the potential energy is at a minimum, r - is the real distance between particles.

Phillip M. Morse proposed this potential function in his 1929 paper to describe the potential energy of diatom molecules, and it is widely used in quantum mechanics and molecular physics to model the vibrational structure of molecules.

The lower and upper limits of the vibrational energy are calculated, the so-called equilibrium distances between atoms in the ground and excited states:

$$r_0(\omega, d, \rho, v) = \rho - 0.3352\frac{\sqrt{D}}{\omega} \cdot log\left\{1 + \frac{0.003651}{D}\sqrt{(0.5+v)\omega(15000D - 750(0.5+v)\omega)}\right\},$$

$$r_1(\omega, D, \rho, v) = \rho - 0.3352\frac{\sqrt{D}}{\omega} \cdot log\left\{1 - \frac{0.003651}{D}\sqrt{(0.5+v)\omega(15000D - 750(0.5+v)\omega)}\right\},$$

also, vibrational energy levels as a function of vibrational quantum number (v):

$$E(\omega, D, v) = 3\omega\left(v + \frac{1}{2}\right) - 0.15\frac{\omega^2}{D}\left(v + \frac{1}{2}\right)^2,$$

and wave function:

$$\Psi(\omega, D, \rho, v, r) = \left(\frac{v!\cdot 3\omega\left(\frac{20d}{\omega}-2v-1\right)}{\sqrt{d}\cdot\Gamma\left(\frac{20d}{\omega}-v\right)}\right)^2 e^{-x/2}x^{10(\mathrm{d}/\omega)-v-1/2}L_v^n(x),$$

which is represented by $\Gamma\left(\frac{20d}{\omega}-v\right)$ – gamma function and Lager polynomial $L_v^n(x)$. $x = \frac{20D}{\omega}e^{-\frac{3\omega}{\sqrt{D}}(r-\rho)}$, $n = \frac{20D}{\omega} - 2v - 1$.

Electronic transitions are described by vibrational processes, which involve simultaneous changes in both vibrational and electronic quantum numbers.

Potential curves of excited electronic states, visualization of vibrational energy levels, and absorption and fluorescence spectra are presented, which reflect the intensity of individual components of vibrational transitions.

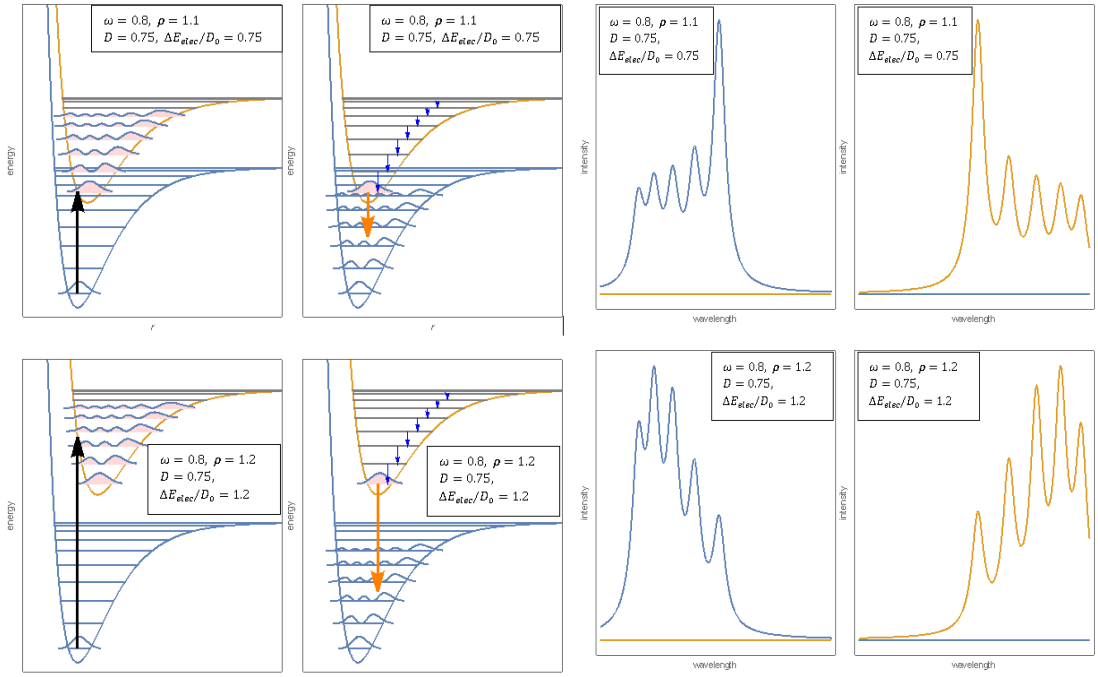

Fig.2.3.1. Absorption (left) and fluorescence (right) potential energy curves of ground and excited electronic states (a) and absorption and excitation spectra (b) for different values of interatomic distance and energy

Fig. 2.3.1 a) presents the basic and excited electronic states with potential energy curves, and Fig. 2.3.1 b) presents the absorption and excitation spectra of the corresponding transitions. These curves illustrate how the potential energy of a molecule varies as a function of interatomic distance. The ground state potential energy curve is usually shown as a blue curve, while the excited state potential energy curve is shown in red.

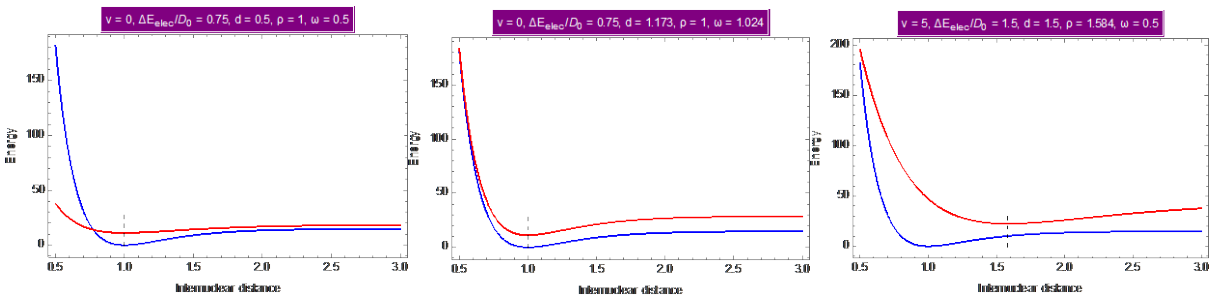

a) b) c)

Fig.2.3.3. Potential energy curves for ground (blue) and excited (red) electronic states

The first graph of Fig. 2.3.3 presents the potential energy curves for the ground (blue) and excited (red) electronic states. The presented visualization allows to determine how the vibrational quantum number (v), electronic energy difference ($\Delta E_{elec}/D_0$), Morse potential depth (D), equilibrium distance (ρ) and frequency (ω) affect the potential energy curves and, accordingly, the spectral transitions of the molecule.

In conclusion, it can be noted that using the Franck-Condon principle, it is explained that the most likely electronic transitions are vertical transitions between potential holes (from the minimum of the ground state to the minimum of the excited state), which is associated with vibration overlap. This causes a change in the vibrational energy level of the molecule and affects the intensity of the vibrational peaks in the spectrum.

The quantum efficiency or sensitivity function for a particular CCD, such as StellarNet's CCD detector in the BlackComet spectrometer, will usually be provided by the manufacturer. It usually varies with wavelength and can be quite complex, often requiring calibration against a light source with a known spectrum. The quantum efficiency curves of the CCD of the BlackComet spectrometer are roughly Gaussian in shape, peaking where the CCD is most sensitive and tapering off towards the edges of its range.

Let's say the CCD sensitivity function in the Black-Comet spectrometer is given by Gaussian form:

$$g(\lambda) = exp\left[\frac{(\lambda - \lambda_0)^2}{2\sigma_\lambda^2}\right]$$

where, λ_0 – is the wavelength (in nm), where CCD sensitivity peaks, λ is the wavelength (nm), σ_λ - standard deviation of the CCD sensitivity curve.

For the simplicity of calculations, let's use the simplified representation of the Franck-Condon factor:

$$FCF(v, v_0) = exp\left[\frac{(v - v_0)^2}{2\sigma_v^2}\right]$$

v_0 – corresponds to the starting point of the vibration propagation of the CCD detector, it actually corresponds to the point of incidence of the light photon, σ_v – reflects the width of the vibrational wave. The signal detection sensitivity of the CCD detector can be calculated by a simplified formula:

$$S_{total}(v, \lambda) = FCF(v, v_0) \cdot g(\lambda).$$

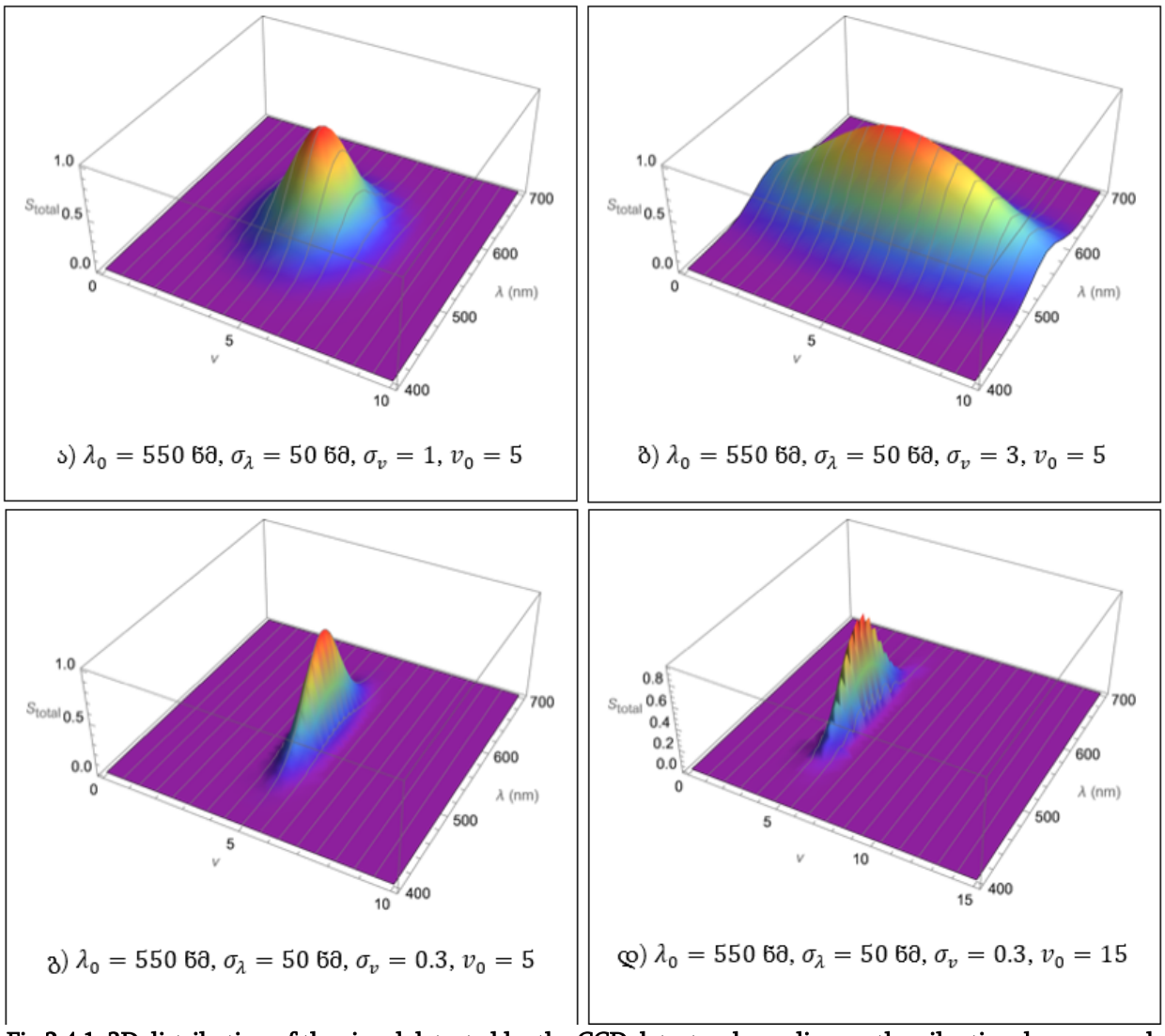

Fig.2.4.1. 3D distribution of the signal detected by the CCD detector depending on the vibrational wave number $v = 1 \ldots 15$ and the wavelength $\lambda = 400 - 700$ nm

In summary, graphical analysis indicates that both molecular characteristics (represented by Franck-Condon factors) and the wavelength sensitivity profile of the CCD play a critical role in determining the detected signal intensity. The graphs presented in Fig. 2.4.1 are unique and can

be used to understand the correlation between molecular spectroscopy and CCD detection capabilities, which will ultimately help to optimize spectroscopic measurements and properly plan experiments.

Chapter III. Modeling CCD characteristics in some practical applications

Main findings: Focusing on diatomic molecules, this section presents a model of electronic transitions involving excited electronic states with higher energy (ΔE_{elec}). This chapter discusses how such transitions are only allowed between certain vibrational levels. The specifics of the electronic transitions and the vibrational changes during these transitions are detailed.

Results: The third chapter of the thesis offers a nuanced understanding of molecular spectroscopy, which is vital to chemical, physical and materials science, especially in contexts where the optical properties of materials are crucial.

§3.1. A quantum harmonic oscillator model for estimating stimulated and spontaneous emission.

The first paragraph of the third chapter of the dissertation includes a bibliographic review of recent advances in fluorescence spectroscopy. The literature review is devoted to articles that describe the practical value of fluorescence spectroscopy in environmental quality assessment, as well as laser-induced plasma fluorescence spectroscopy, and the possibility of spectral line prediction based on the Franck-Condon principle.

The quantum harmonic oscillator model for estimating stimulated and spontaneous radiation is discussed.

As known, quantum mechanics describes energy as quantized, meaning that atoms and molecules exist in discrete energy states. Photons, which are quanta of light, can interact with atoms, causing electronic transitions between these states: $\hbar\omega = E_1 - E_0$

Three types of transitions are possible when this resonance condition is met:

- **Absorption:** An atom moves from a lower energy state to a higher energy state by absorbing a photon.
- **Stimulated emission:** The incident photon causes the atom to move from a higher energy state to a lower energy state, releasing a photon of the same energy.

- **Spontaneous emission:** An atom spontaneously moves from a higher energy state to a lower energy state and emits a photon.

The quantum harmonic oscillator model describes well the behavior of photons in the field. Probability of photon annihilation (decrease of photon number by one): $|\langle n_\omega - 1|a_\omega|n_\omega\rangle|^2 = n_\omega$, or the probability of photon generation (increasing the photon number by one): $|\langle n_\omega + 1|{a_\omega}^+|n_\omega\rangle|^2 = n_\omega + 1$ ვdefines the quantum-mechanical basis of the photon. a_ω and ${a_\omega}^+$ - are photon annihilation and generation operators, and n_ω - is the number of photons.

§3.2. Estimation of light power transmission coefficient in biological tissues. This paragraph is devoted to the theoretical analysis of light scattering in biological tissues. It is specifically concerned with the estimation of the light transmission coefficient in biological tissues, such as erythrocytes in the blood or polarized molecules of the skin membrane.

The case is considered when light affects a biological structure, for example, polarized molecules of blood erythrocytes or body skin membrane. It is noted that in this case the dominant effect is light scattering and absorption. Scattered radiation propagation is described by the photon transfer equation:

$$(\vec{S}\cdot\nabla)\vec{L}(r,\vec{S}) = \frac{d\vec{L}}{dS} = -\alpha_t L(r,\vec{S}) + \alpha_s \int_{4\pi} \vec{P}(\vec{S},\vec{S}')\vec{L}(r,\vec{S}')d\vec{S}$$

P (w)- is the power of the incident beam, R (mm) – is the radius of the spot produced by the ray at the point of incidence of the ray, $\vec{L}(r,\vec{S})$ (mw/mm²·sr) - is the rate of change of brightness at the point $r(x,y,z)$, which is located in the $\vec{S}$ direction. The direction of light incidence is $\vec{S}'$.
We can expand the plane waves according to the Legendre polynomial and find the expression of the perturbation amplitude and the differential perturbation rate:

$$\frac{d\sigma}{d\Omega} = \frac{1}{k^2}\left|\sum_{l=0}^{\infty}(2l+1)e^{i\delta}\cdot\sin(\delta)\cdot L_l(\cos(\theta))\right|^2$$

These equations are needed to calculate the depth of light penetration in biological tissues:

$$S(\lambda,P,\delta,d)\sim\frac{P}{4\pi\delta^2}\exp\left[-\left(\frac{\sin(0.5)}{\lambda}\right)^2+\frac{d}{\delta}\right],$$

Where, P - is the power of the light source at λ - wavelength, δ - is the optical thickness of the biological tissue, d the depth of light penetration into the biological tissue. The exponential part indicates that the power factor $S(\lambda, P, \delta, d)$ decreases with increasing scattering angle and depth, but increases towards longer wavelengths.

In order to simplify the calculations, several assumptions are made: it is assumed that the scattering is elastic, the effect of multiple scattering is neglected, and the thickness of the light flux is such that the bioparticles have a definite momentum.

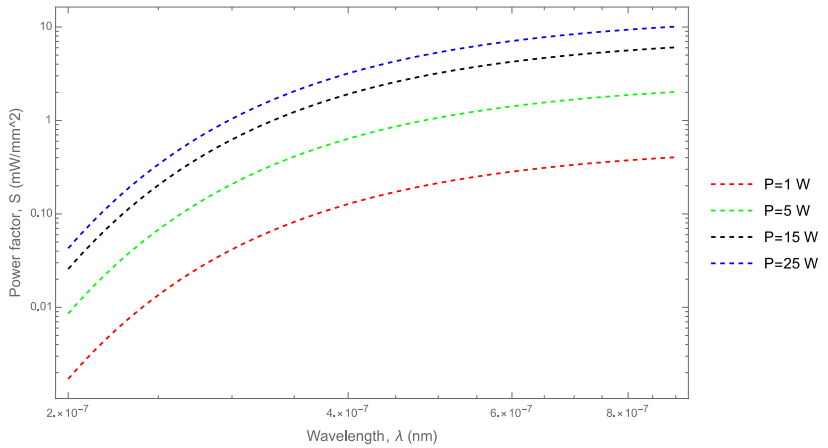

Fig.3.2.1. Dependence of the coefficient of light power penetrating into biological structures on the wavelength in log-log scale for different power sources

The curves generally show that as the wavelength increases, the power factor decreases. Less energy is delivered to the biological structure at higher wavelengths due to increased scattering, or possibly due to source characteristics. It is also noticeable that the power factor increases with the source power settings. This means more energy is delivered at higher power, which is expected.

For diatomic molecules, electronic transitions often occur with vibrational and rarely with rotational energies. Therefore, these transitions have a selective character. However, rotational energies in liquids are often negligible due to the rapid motion of molecules, so we may consider only vibrational transitions in liquids. Curves of potential energies at the ground and excited energy levels and associated vibrational wave functions provide characteristic vibrational spectra.

§3.3. Evaluation of CCD sensor sensitivity in its use in biological applications. The third paragraph of the third chapter of the thesis is devoted to the assessment of the sensitivity of the CCD sensor for biological applications. It outlines the technical details of how a CCD sensor

detects light and converts it into an electrical signal. It deals with the interaction of light with biological tissues, including how various factors such as light source power, wavelength, and tissue optical depth affect the sensor's response. The spectral response of CCD sensors is its sensitivity as a function of wavelength:

$$R(\lambda) = QE(\lambda) \cdot S(\lambda, P, \delta, d)$$

The sensitivity of the CCD sensor in its use in biological applications is evaluated.

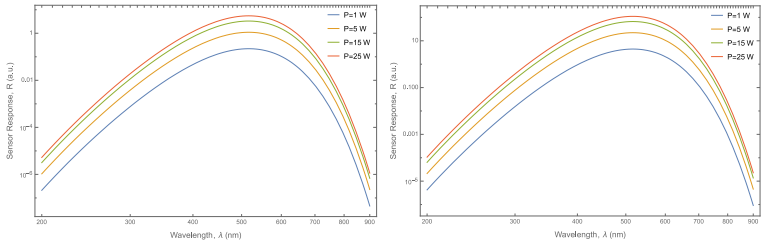

Fig.3.2.2. Dependence of CCD-sensor sensitivity $R(\lambda)$ on the wavelength after light passes through the biological structure, when $\delta = 1$ mm, a) $d = 1$ mm, b) $d = 2$ mm, In the case of different power P of the light source, $\lambda_0 = 500$ nm.

Fig. 3.2.2 shows the dependence of the CCD sensor sensitivity $R(\lambda)$ (the same echo) on the wavelength after passing the light through the biological structure, when the optical thickness of the biological tissue is $\delta = 1$ mm, and the depth of light penetration into the biological tissue is changed to $d = 1$ mm (Fig. 3.2.2 a), $d = 2$ mm (Fig. 3.2.2 b), in the case of different power P of the light source. Modeling is done in the case of the Gaussian dependence of the quantum efficiency QE of the CCD-sensor on the wavelength, when the light source is centered at the wavelength $\lambda_0 = 500$ nm, and Fig. 3.2.3 a) and b) present similar graphs of the quantum efficiency QE in the Gaussian distribution depending on the wavelength , when the light source is centered at the wavelength $\lambda_0 = 500$ nm.

The discussion suggests that CCD sensor performance can be optimized for specific applications by selecting the QE peak of the sensor to match the wavelength of interest for the study. This will allow us to obtain the best possible signal-to-noise ratio and thereby increase the efficiency of the sensor for specific biological imaging or analytical purposes.

§3.4. Evaluation of CCD sensor signal-to-noise ratio in its use in biological applications. In this section, the signal-to-noise ratio (SNR) of CCD sensors for biological applications is investigated. It considers the dynamic range of CCD sensors, which is defined by the maximum signal that can be recorded (full capacitance) to the minimum detectable signal (usually read noise).

The performance of the sensor is investigated by simulation analysis. SNR is significantly dependent on the relationship between the system parameters: sensor peak sensitivity

wavelength, integration time, light penetration depth and optical depth in biological tissue. These results highlight the importance of determining and accounting for the QE peak of the sensor. An increase in the signal-to-noise level of the sensor may require a longer integration time or more sensitive equipment (given the specific design and construction).

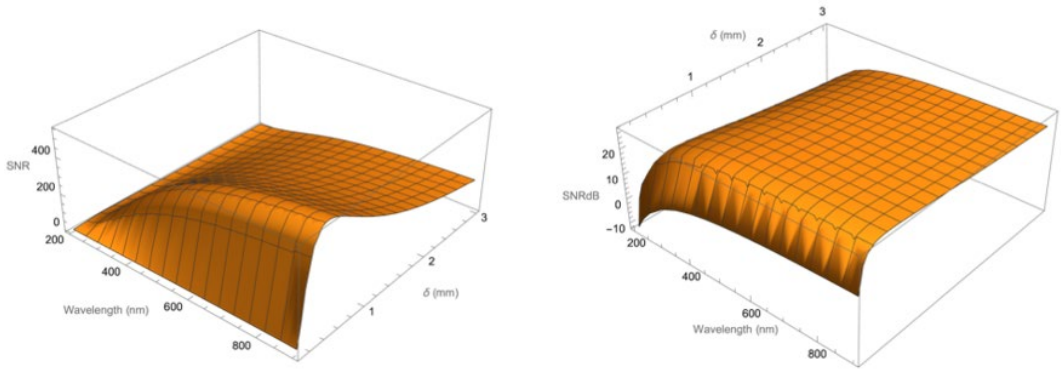

Fig.3.4.1. Dependence of signal-to-noise ratio on wavelength (λ) and optical depth (δ) when $\lambda_0 = 500$ nm, integration time t=100 s, and light penetration depth in biological tissues d=1 mm

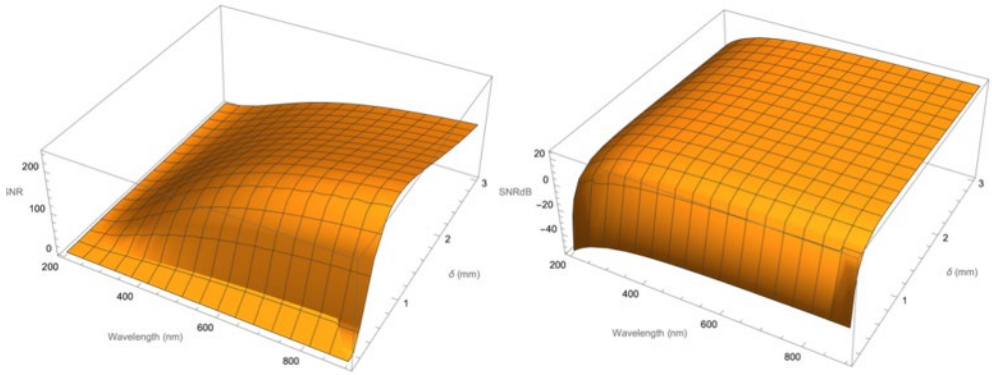

Fig.3.4.2. Dependence of signal-to-noise ratio on wavelength (λ) and optical depth (δ) when$\lambda_0 = 200$ nm, integration time t=100 s, and light penetration depth in biological tissues d=2 mm

As a result, we can draw several important conclusions:

- When λ_0=500 nm, t=100 s and d=1 mm: SNR decreases with increasing wavelength. This is an expected result, as sensor sensitivity generally decreases at wavelengths far from the peak sensitivity (λ_0). The SNR also decreases with increased optical depth, δ, reflecting the decrease in signal power with increasing penetration depth.
- When λ_0=500 nm, t=100 s and d=2 mm: a similar trend is observed with decreasing SNR for higher wavelengths and larger optical depths. An increase in the depth (d) of the biological tissue leads to a decrease in the low SNR in the entire wavelength range, which allows us to assume that the ability of the sensor to distinguish signal from noise decreases, and the decrease in this ability becomes more pronounced when the light penetrates deeper into the depths of the biological tissue.

- When λ_0=200 nm, t=100 s: increasing the light penetration depth in the biological structure from d=1 mm to d=2 mm shows that the peak sensitivity shifts to a shorter wavelength (200 nm), the behavior of the SNR curve changes significantly . The SNR is higher at shorter wavelengths, which corresponds to a peak quantum efficiency (QE) value near 200 nm. However, the SNR continues to decrease with increasing optical depth (δ).

§3.5. Estimation of the signal-to-noise ratio in the absorption spectrum of cold atoms. The fifth paragraph of the third chapter of the thesis evaluates the signal-to-noise ratio (SNR) in the context of cold atom absorption spectroscopy.

The signal-to-noise ratio in the absorption spectrum of cold atoms is estimated. Fig. 3.5.1 shows the dependence of SNR on the number of incident photons C_{in} when the optical density (OD) of the sample, the effective saturation index of the detector (C_{sat}^{eff}) and the exposure time (τ) are changed.

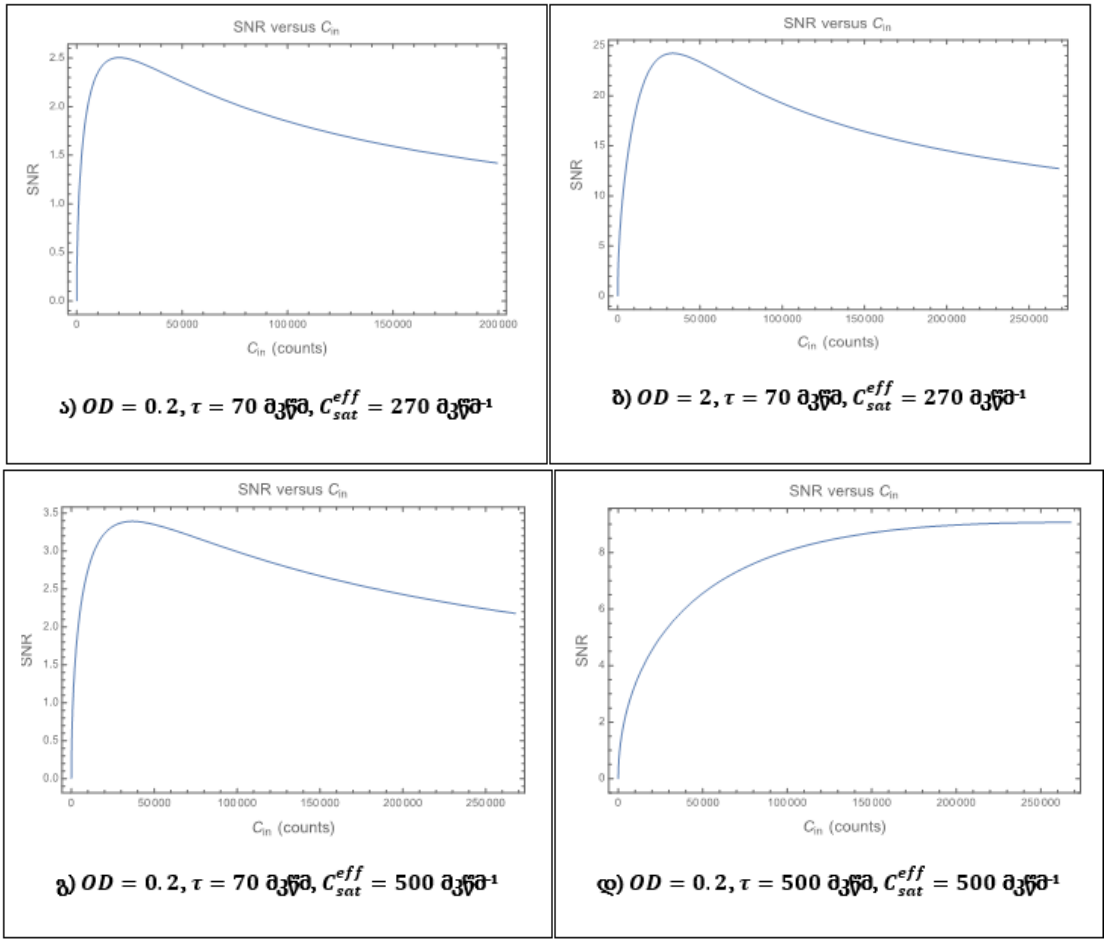

Fig.3.5.1. Dependence of the signal-to-noise ratio (SNR) on the number of incident photons, when the noise coefficient $ND = 0.6$, the electron multiplication coefficient G=6.5, for different sample optical density (OD), exposure time (τ) and the effective saturation index of the detector (C_{sat}^{eff})

From the analysis of the graphs, we determine that:

- When the optical density (OD) and CCD-detector effective saturation (C_{sat}^{eff}) are small, the signal-to-noise ratio SNR shows a practically peak value, but stabilizes quickly, indicating that the detector rapidly reaches its maximum capability with increasing photon number.
- The increase in optical density affects the signal-to-noise ratio, which is explained by the absorption of the signal by the sample. The high optical density (OD) of the sample results in fast signal transmission and thus a reduction in the signal-to-noise ratio.
- An increase in the effective saturation index (C_{sat}^{eff}) of the CCD-detector leads to an increase in the signal-to-noise ratio (SNR) over a wider range, practically up to saturation. This indicates that detectors with a high saturation factor (C_{sat}^{eff}) process more photons.

§3.6. Methods of Analytical-Statistical Processing of Excitation/Emission Spectral Data in Wine Spectroscopy Applications. The study includes fluorescence spectroscopy excitation/emission matrix (AEM) analysis, peak component analysis (PCA) and tolerance sample comparison analysis (TES) method development and modeling according to wine product variety and origin. About 100 samples of four types of white Georgian wine were taken. The methodology chosen by us is based on the one hand on the hardware complex, which was gradually modernized by our group, on the other hand on the development of new analytical approaches, which are quite acceptable to be used in typical laboratory control of food products and beverages.

Fluorescence spectra were recorded using a Black Comet (200-950 nm) spectrometer manufactured by StellarNet. LED lamps of different frequencies were used as light sources. A wine sample of 100 μl is placed in a quartz cuvette and the spectra are recorded at room temperature. The number of scans is determined from the same experimental measurement to exclude drift effects on the sample. At the beginning of each experiment, the standard is calibrated. The excitation wavelength range is between 250-500 nm, and the emission wavelength is between 275-600 nm. Measurements are performed at different excitation wavelengths with a 5 nm bias. The wavelength system is calibrated each day according to the combined scattering (Raman scattering) peak to account for possible instrument wavelength drift. The total time to scan a sample is approximately 10 minutes. Measurements were performed over

a short period of time (10-15 days), thereby minimizing the influence of atmospheric effects and instrumental fluctuations (ex. lamp intensity fluctuations).

In order to process excitation-emission spectral data, the excitation/emission wavelengths of N samples must be placed in a three-dimensional array of size $i \times j \times k$, where i is the number of samples, j is the number of emission wavelengths, k is the number of excitation wavelengths:

$$x_{ijk} = \sum_{n=1}^{N} a_{in} b_{jn} c_{kn} + e_{ijk}$$

Using PCA analysis, we built tables and graphs for a specific group of samples.

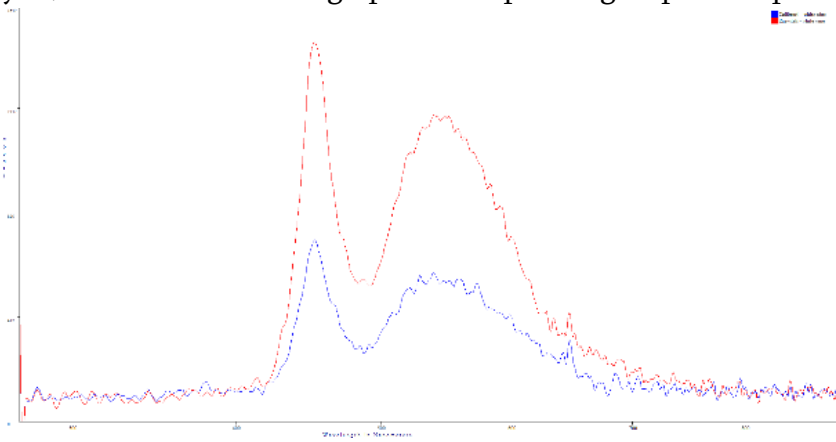

Fig. 3.6.1. Emission spectra of Georgian white wine: Tsolikauri (blue), Rkatsiteli (red).

In processing the wine spectrum, we used multivariate analysis techniques (PARAFAC) such as PCA (Principal Component Analysis) to highlight the main features of the data. We performed statistical analysis of the data to identify patterns or differences between different wine samples. Our conclusions mainly concern the measuring device. These results refer to the CCD-detectors of the BlackCommet spectrometers manufactured by StellarNet, namely:

1. The spectra show a larger change in the average signal level at a given integration time, possibly due to thermal fluctuations between measurements. Therefore, the optimal level of thermal stabilization was selected for the spectrometer. As the measurements showed, to achieve thermal stabilization, the average signal level should be calculated with about 100 integrations in 180 milliseconds.
2. One of the main features of the spectrometer is the so-called "dark current" which averages about 0.25% of the peak value (~40,000 photons, with 100 integrations). These data were calculated in the combined spectrum of the deuterium and halogen light sources.

3. Data collected during various integrations show that until the integration time is increased to ~2000 msec, digital data acquisition of the signal continues. Further increasing the integration time leads to an approximately linear increase in the dark current.

Conclusion

Modeling the electronic transitions and 3D analysis of the detected signal show that when molecules absorb or emit light, they can transition between different energy states. The Franck-Condon principle provides a means of predicting the intensity of spectral lines in absorption and emission spectra. It states that electronic transitions are so fast compared to nuclear motion that the nuclei are effectively stationary during the transition. Thus, the most intense transitions are those where the vibrational wavefunctions of the initial and final electronic states have the greatest overlap. Franck-Condon factors are numerical values that represent the probability of transitions between vibrational levels in different electronic states. These factors depend on the square of the integral of the overlap of the vibrational wave functions of the initial and final states.

In spectroscopy, a CCD sensor is used to capture the spectral distribution of light emitted or absorbed by a sample. The quantum efficiency (QE) determines how well a CCD captures light, and it can vary depending on the wavelength of the light.

When a sample is irradiated with light in a spectroscopic experiment, the intensity of emitted or absorbed light at different wavelengths is modulated by Franck-Condon factors, which are then detected by the CCD. Therefore, the total signal captured by the CCD ($S_{total}(v, \lambda)$) will be affected by both the intrinsic spectral properties of the sample (via quantum mechanics and the Franck-Condon principle) and the technical characteristics of the CCD (such as its QE at different wavelengths).

From the results of evaluating the sensitivity of the CCD sensor, we can make a number of conclusions about the possibility of increasing the sensitivity of the sensor:

1. The QE curve is Gaussian meaning that the sensor has peak sensitivity at a specific wavelength (which represents the center of the Gaussian). In our case, the QE peak was centered at 500 nm and 300 nm in the simulation. A sensor will be most efficient at converting incident photons into an electronic signal near these peak wavelengths.

2. We studied the response of the sensor at different values of light source power (1 W, 5 W, 15 W and 25 W). As the power increases, so does the response of the sensor. This is because a higher power level means more photons hitting the sensor are correspondingly converted into electrons.
3. When the optical density (OD) and CCD-detector effective saturation (C_{sat}^{eff}) are small, the signal-to-noise ratio SNR shows a practically peak value, but stabilizes quickly, indicating that the detector rapidly reaches its maximum capability with increasing photon number.
4. The signal-to-noise ratio (SNR) increases with the increase of the saturation index (C_{sat}^{eff}) up to a certain point, which is a typical property of CCD detectors, because the increase in signal intensity uniquely contributes to the improvement of the SNR until noise or other technical factors (detector threshold) will not limit it.

Using CCD-detectors of BlackCommet spectrometers manufactured by StellarNet in wine applications, we find that:

- The spectra show a larger change in the average signal level for a given integration time, possibly due to thermal fluctuations between measurements. Therefore, the optimal level of thermal stabilization was selected for the spectrometer. As the measurements showed, to achieve thermal stabilization, the average signal level should be calculated with about 100 integrations in 180 milliseconds.
- One of the main features of the spectrometer is the so-called "dark current", which averages about 0.25% of the peak value (~40,000 photons, with 100 integrations). These data were calculated in the combined spectrum of the deuterium and halogen light sources.
- Data collected during various integrations show that until the integration time is increased to ~2000 msec, digital data collection of the signal continues. Further increasing the integration time leads to an approximately linear increase in the dark current.
- Variation of the integration time reveals fixed pattern noise peaks in the recorded spectrum: when the integration time is <150 msec, there is a decrease in the dark current

and it corresponds to a wavelength of 717.5 nm; Integration times >500 msec reveal two significant dark current peaks at wavelengths of 717.5 nm and 666.6 nm.

It should be noted that these observations undoubtedly provide useful results for the optimization of detector performance. The results are important for choosing the appropriate measurement parameters and setting up the experiments correctly to avoid detector saturation, which limits the achievement of the maximum SNR value.

The thesis emphasizes the importance of high-level analytical control to ensure the success of production processes and the development of modern technologies. When we delve into the optical methods available for the chemical analysis of the environment, the need to select and optimally adapt these methods to the specific properties of the investigated substances appears as a crucial task.

Thus, the thesis not only contributes to the development of knowledge in optical analysis, but also sets the stage for future innovations in the field, and contributes to the constant need for accuracy, adaptability and improvement of analytical technologies.

The results obtained in the doctoral thesis are presented in the following scientific articles:

1. **Shainidze J.J.**, Gomidze N.Kh., Optimizing QE of CCD by Modifying BlackComet Detector Program. XII Japanese-Mediterranean Workshop on Applied Electromagnetic Engineering for Magnetic Superconducting, Multifunctional and Nanomaterials, 2023
2. **Shainidze J.J.**, Gomidze N.Kh., Creating Fluorescence Spectra Based on The Franck-Condon Factor. 66th International Conference for Students of Physics and Natural Sciences – Open Readings, 2023
3. Khajishvili M., **Shainidze J.**, Makharadze K. & Gomidze N. On the development of the fluorescence excitation-emission etalon matrix algorithm of wine. The Eurasia Proceedings of Science, Technology, Engineering & Mathematics (EPSTEM), 2023
4. Khajishvili M.R., Gomidze N.Kh., **Shainidze J.J.**, Estimation SNR of CCD camera for OD medium. International Conference on Basic Sciences, Engineering and Technology (ICBASET), 2022

5. Khajishvili M.R., Gomidze N.Kh., **Shainidze J.J.**, 3D Fluorescence Spectroscopy of Liquid Media via Internal Reference Method, Research and Education: Traditions and Innovations, 2022
6. Gomidze N.Kh., **Shainidze J.J.**, Jabnidze I., Makharadze K., Khajishvili M., Kalandadze L., Nakashidze O., Mskhaladze E., Estimation of Scintillation Index on a superconductor receiver for Gaussian Laser Beam propagated through Random Phase Screen. Journal of Biological Physics and Chemistry, 2020
7. **Shainidze J.**, Kalandadze L., Nakashidze O., Gomidze. N., Estimation of parameters for a model of polycrystalline solar cells. Nanotechnology and Perceptions vol. 16, 2020
8. **Shainidze J.**, Gomidze N., Shengelia G., Turmanidze R., To the problems of fluorescence excitation spectrums. International scientific journal "Machines. Technologies. Materials.", 2018

References

[1] დიმიტრაძე მ. (2020) შემთხვევითად - არაერთგვაროვანი ფაზური ეკრანის ლაზერულ ფლუორესცენციული სპექტროსკოპია. სამაგისტრო ნაშრომი, ბსუ.

[2] მაჭავარიანი ზ. (2018). *ატომური ფიზიკა.* თსუ, ISBN 978-9941-13-722-8 (pdf)

[3] ღომიძე ნ., ღომიძე ხ. (2022) *რადიოფიზიკა.* ISBN 978-9941-488-57-3. UDC(უაკ)621.39(075.8)ღ-796. https://rustaveli.org.ge/geo/200916031925tsignebi/radiofizika

[4] ღომიძე ნ., ჯაბნიძე ი., სურმანიძე ზ. (2023) *ფიზიკური პროცესების მოდელირება,* ISBN 978-9941-488-72-6, UDC(უაკ) 53(075.8) ღ-792023

[5] Alia, J. D., & Flack, J. A. (2020). Unspecified verticality of Franck–Condon transitions, absorption and emission spectra of cyanine dyes, and a classically inspired approximation. RSC advances, 10(70), 43153-43167.

[6] Arnone, R. A., & Parsons, A. R. (2005). Real-time use of ocean color remote sensing for coastal monitoring. In Remote Sensing of Coastal Aquatic Environments: Technologies, Techniques and Applications (pp. 317-337). Dordrecht: Springer Netherlands.

[7] Azcarate S. M. et al. Modeling excitation–emission fluorescence matrices with pattern recognition algorithms for classification of Argentine white wines according grape variety. Food Chem. 184, 214–219 (2015).

[8] Batsaikhan, M., Ohba, H., Karino, T., Akaoka, K., & Wakaida, I. (2024). Simultaneous analysis of gadolinium and surface imaging using a fiber-coupled acoustic wave-assisted microchip LIBS system. Journal of Analytical Atomic Spectrometry, 39(2), 423-432.

[9] Bautz, M., Foster, R., LaMarr, B., Malonis, A., Prigozhin, G., Miller, E., ... & Suntharalingam, V. (2018, July). Toward fast low-noise low-power digital CCDs for Lynx and other high-energy astrophysics missions. In Space Telescopes and Instrumentation 2018: Ultraviolet to Gamma Ray (Vol. 10699, pp. 238-248). SPIE.

[10] Birks J., Munro I. The Fluorescence Lifetimes of Aromatic Mole cules, Progress in Reaction Kinetics, vol. 4, Pergamon Press, Oxford, 196

[11] Blinder S. M. (2004). *Introduction to Quantum Mechanics*, Amsterdam: Elsevier, pp. 229–232

[12] Born, M. (1927). Born-oppenheimer approximation. Ann. Phys, 84, 457-484.

[13] Bromley, S. J., Noonan, J. W., Cochran, A. L., Stachová, B., Országh, J., Ivanova, O., ... & Bodewits, D. (2024). An updated fluorescence emission model of CO+ for cometary science. Monthly Notices of the Royal Astronomical Society, stae456.

[14] Cappai, A., Melis, C., Stagi, L., Ricci, P. C., Mocci, F., & Carbonaro, C. M. (2021). Insight into the Molecular Model in Carbon Dots through Experimental and Theoretical Analysis of Citrazinic Acid in Aqueous Solution. The Journal of Physical Chemistry C, 125(8), 4836-4845.

[15] Chang J.L. A new method to calculate Franck–Condon factors of multidimensional harmonic oscillators including the Duschinsky effect, J. Chem. Phys. 128 (2008) 174111-1–174111-12. https://doi.org/10.1063/1.2916717.

[16] Chen, L., Zhang, X., Lin, J., & Sha, D. (2009). Signal-to-noise ratio evaluation of a CCD camera. Optics & Laser Technology, 41(5), 574-579.

[17] Dahm, D., Dahm, K. (2007). Interpreting Diffuse Reflectance and Transmittance: A Theoretical Introduction to Absorption Spectroscopy of Scattering Materials. doi:10.1255/978-1-901019-05-6. ISBN 9781901019056

[18] Daily, J. W. (1997). Laser induced fluorescence spectroscopy in flames. Progress in energy and combustion science, 23(2), 133-199.

[19] Davenport, J. J., Hodgkinson, J., Saffell, J. R., & Tatam, R. P. (2015). Noise analysis for CCD-based ultraviolet and visible spectrophotometry. Applied Optics, 54(27), 8135-8144.

[20] Davitadze Z., Gomidze N., Makharadze K. Control Laser Spectrofluorimeter with Microcontrollers. Journal of Advanced Materials Research Vol. 590 (2012), pp. 201-205. www.scientific.net/AMR.590.206

[21] De Filippis, G., Cataudella, V., Mishchenko, A. S., Perroni, C. A., & Devreese, J. T. (2006). Validity of the Franck-Condon principle in the optical spectroscopy: optical conductivity of the Fröhlich polaron. Physical review letters, 96(13), 136405.

[22] De la Viuda-Pérez, I., Navarro-Azor, R., Lalla, E. A., Rodríguez-Losada, J. A., Aquilano, R., Medina, J., & Rull-Pérez, F. (2016). Studies of Basalt Through Laser Induced Breakdown Spectroscopy (LIBS) for the Manufacturing of Lapilli Blocks. Minería y Geología, 32(3), 78-95.

[23] Devanesan, S., AlQahtani, F., AlSalhi, M. S., Jeyaprakash, K., & Masilamani, V. (2019). Diagnosis of thalassemia using fluorescence spectroscopy, auto-analyzer, and hemoglobin electrophoresis—A prospective study. Journal of Infection and Public Health, 12(4), 585-590.

[24] di Frischia, S., Chiuri, A., Angelini, F., & Colao, F. (2018, November). Optimization of signal-to-noise ratio in a CCD for spectroscopic applications. In 15th European Workshop on Advanced Control and Diagnosis (pp. 439-452). Cham: Springer International Publishing.

[25] Doležal, J., Canola, S., Hapala, P., de Campos Ferreira, R. C., Merino, P., & Švec, M. (2022). Evidence of exciton-libron coupling in chirally adsorbed single molecules. Nature communications, 13(1), 6008.
[26] Duschinsky F. On the interpretation of electronic spectra of polyatomic molecules. I. The Franck-Condon principle, Acta Physicochim. URSS 7 (1937) 551–566.
[27] Eisenthal K.B., Chem. Phys. Letters, 6, 155 (1970)
[28] G. Reinaudi, T. Lahaye, Z. Wang and D. Guéry-Odelin, "Strong Saturation Absorption Imaging of Dense Clouds of Ultracold Atoms," Optics Letters, 32(21), 2007 pp. 3143\[Dash]3145. doi:10.1364/ol.32.003143.
[29] GE Health Care. ÄKTA Laboratory-Scale Chromatography Systems - Instrument Management Handbook. GE Healthcare Bio-Sciences AB, Uppsala, 2015. https://cdn.gelifesciences.com/dmm3bwsv3/AssetStream.aspx?mediaformatid=10061&destinationid=10016&assetid=16189.
[30] Georgieva, I., Kossev, K., Titorenkova, R., Petrova, N., Zahariev, T., & Nikolova, R. (2022). Effect of urea on arrangement of novel Mg (II) perrhenate crystal structures and their optical properties: Experimental and theoretical insight. Journal of Solid State Chemistry, 312, 123263.
[31] Gevin, O., Limousin, O., & Meuris, A. (2016, July). Front-end ASICs for high-energy astrophysics in space. In Space Telescopes and Instrumentation 2016: Ultraviolet to Gamma Ray (Vol. 9905, pp. 177-191). SPIE.
[32] Gewali, U. B., Monteiro, S. T., & Saber, E. (2018). Machine learning based hyperspectral image analysis: a survey. arXiv preprint arXiv:1802.08701.
[33] Gomidze N. Kh, Khajisvili M. R., Jabnidze I. N., Makharadze K. A., Surmanidze Z. J. To the Problems of Detecting Signals Passing Through a Random Phase Screen. Journal "Recent Advances in Technology Research and Education" Springer International Publishing. Print ISBN: 978-3-319-99833-6, Electronic ISBN: 978-3-319-99834-3, pp. 177-184, 2018.
[34] Gomidze N., Shainidze J., Shengelia G., Turmanidze R. To the problems of fluorescence excitation spectrums. International scientific journal "machines. Technologies. Materials." web ISSN 1314-507X; print ISSN: 1313-0226, pp.279-282, 2018.
[35] Gomidze N., Jabnidze I., Makharadze K., Khajishvili M., Shashikadze Z., Surmanidze Z., Surmanidze I. Numerical Analyses of Fluorescence Characteristics of Watery Media via Laser Spectroscopy Method. Journal of Advanced Materials Research Vol. 590 (2012), pp. 206-211. www.scientific.net/AMR.590.201
[36] Gomidze N.Kh, Shashikadze Z.Kh., Makharadze K.A., Khajishvili M.R. About fluorescence excitation spectrums. 6th International Conference on Advanced Optoelectronics and Lasers. Conference Proceedings. 9-13 September (2013), Sudak, Ukraine, pp. 317-319.
[37] Gomidze N.Kh., Jabnidze I.N., Surmanidze Z.J. Stroboscopic Method of Fluorescence Analyses of Optically Solid Media. 2016 IEEE 7th International Conference on Advanced Optoelectronics and Lasers (CAOL). September 12-15, Odessa, Ukraine, pp. 34-36, 2016.
[38] Gomidze N.Kh., Makharadze K.A., Khajishvili M.R., Jabnidze I.N., Shashikadze Z.Kh. Some Issues of Fluorescence Characteristics Aqueous Media via Diagnosis of Laser Spectroscopy Method. International Journal of Engineering, Science and Innovative

Technology. ISSN No: 2319-5967 (ISO 9001:2008 Certified, Impact Factor of IJESIT is 1.753), №3, issue 3, pp.142-152, 2014.

[39] Gomidze N.Kh., Shainidze J.J., Jabnidze I.N., Makharadze, K.A., Khajishvili M.R., Kalandadze L.G., Nakashidze O, Mshkhaladze E.N. Estimation of scintillation index for a Gaussian laser beam propagating through a random phase screen. Journal of Biological Physics and Chemistry, Vol. 20 (2020), doi: 10.4024/27GO19A.jbpc.20.03.

[40] Gomidze N.Kh., Shainidze J.J., Khajishvili M.R., Jabnidze I.N., Makharadze K.A., Kalandadze L.G., Nakashidze O.M., Surmanidze Z,J., Mskhaladze E.N., Gomidze L.N. 3D fluorescence spectroscopy to study the distribution of bioparticles. International Scientific Conference Modern Research Methods of Bio-Nano-Agents, 24-26 November, pp.21-27, BSU, Batumi. ISBN: 978-9941-488-46-7

[41] Gritchenko, A. S., Eremchev, I. Y., Naumov, A. V., Melentiev, P. N., & Balykin, V. I. (2021). Single quantum emitters detection with amateur CCD: Comparison to a scientific-grade camera. Optics & Laser Technology, 143, 107301.

[42] Guyon F., Magdas A. Application of fluorescence spectroscopy using classical right angle technique in white wines classification. (2019).

[43] Han, S. (2019). Utility analysis for optimizing compact adaptive spectral imaging systems for subpixel target detection applications. Rochester Institute of Technology.

[44] He, Y., Ott, C., Pfeifer, T., & Gaarde, M. B. (2024). Local enhancement in transient absorption spectroscopy by gating the resonance in the time domain. Physical Review Research, 6(1), 013103.

[45] Henrichs, C., Hebestreit, M. L., Krügler, D., & Schmitt, M. (2020). Structural changes upon electronic excitation in 1, 2-dimethoxybenzene from Franck-Condon fits of the fluorescence emission spectra. Journal of Molecular Structure, 1211, 127855.

[46] Hoppe, W., Lohmann, W., Markl, H., Ziegler, H. Biophysics, New York: Springer-Verlag, 1983.

[47] Hossain, A. (2023). Spectral simulation and method design of camouflage textiles for concealment of hyperspectral imaging in UV-Vis-IR against multidimensional combat background. The Journal of the Textile Institute, 114(2), 331-342.

[48] Hossain, M. A. (2021). Adaptive camouflage textiles with thermochromic colorant and liquid crystal for multidimensional combat background, a technical approach for advancement in defence protection. American Journal of Materials Engineering and Technology, 9(1), 31-47.

[49] Ikeda, Y., Soriano, J. K., & Wakaida, I. (2022). Signal-to-noise ratio improvements in microwave-assisted laser-induced breakdown spectroscopy. Talanta Open, 6, 100138.

[50] Inochkin, F., Kruglov, S., & Bronshtein, I. (2016, February). Increasing CCD frame rate and signal-to-noise ratio with high resolution capability using on-chip preprocessing and multisignal image representation. In 2016 IEEE NW Russia Young Researchers in Electrical and Electronic Engineering Conference (EIConRusNW) (pp. 209-213). IEEE.

[51] Ishizawa, S., Kurosawa, S., Kurashima, Y., Kodama, S., Morishita, Y., Yamaji, A., ... & Tanaka, H. (2023). Optical and scintillation properties of Yb-doped La2Hf2O7 crystal grown by core heating method for fiber reading remote-dosimetry system. Optical Materials, 142, 113941.

[52] Ishizawa, S., Kurosawa, S., Kurashima, Y., Kodama, S., Morishita, Y., Yamaji, A., ... & Tanaka, H. (2023). Optical and scintillation properties of Yb-doped La2Hf2O7 crystal

grown by core heating method for fiber reading remote-dosimetry system. Optical Materials, 142, 113941.

[53] IUPAC, Compendium of Chemical Terminology, 2nd ed. (the "Gold Book") (1997). Online corrected version: (2006–) "decadic absorbance". doi:10.1351/goldbook.D01536

[54] Ji, C., Xu, H., Yu, H., Cui, Z., Fan, J., & Zhai, Z. (2024). An online monitoring device for measuring the concentration of four types of in-situ microorganisms by using the near-infrared band. Spectrochimica Acta Part A: Molecular and Biomolecular Spectroscopy, 310, 123895.

[55] Kanou, M., Kameoka, T., Suehara, K. I., & Hashimoto, A. (2017). Mid-infrared spectroscopic analysis of saccharides in aqueous solutions with sodium chloride. Bioscience, Biotechnology, and Biochemistry, 81(4), 735-742.

[56] Kastrati, A., Oswald, F., Scalabre, A., & Fromm, K. M. (2023). Photophysical Properties of Anthracene Derivatives. Photochem, 3(2), 227-273.

[57] Khajishvili M., Gomidze N., Shainidze J. Estimation SNR of CCD camera for OD medium. The Eurasia Proceedings of Science, Technology, Engineering & Mathematics (EPSTEM). ISBN:978-605-73797-9-5 ISSN: 2602-3199, Publication date: 2022, Pages: 130-138.

[58] Khajishvili M., Shainidze J., Makharadze K. & Gomidze N. (2023). On the development of the fluorescence excitation-emission etalon matrix algorithm of wine. The Eurasia Proceedings of Science, Technology, Engineering & Mathematics (EPSTEM), 23, 93-99.

[59] Khajishvili, M., Gomidze, N., Jabnidze, I., Makharadze, K., Kalandadze, L., & Nakashidze, O. (2023). CREATION 3D FLUORESCENCE SPECTRA OF WINE. Book of Abstracts JAPMED, 12, 100-102.

[60] Khajisvili M.R., Gomidze N.Kh, ShainidzeJ.J. 3D Fluorescence Spectroscopyof Liquid mediavia internal reference method. INTER-ACADEMIA 2021: Research and Education: Traditions andInnovations, Partof the Lecture Notes in Networks and Systems book series (LNNS,volume 422,pp.59-71). DOI: 10.1007/978-981-19-0379-3_7.

[61] Khajisvili, M. R., Gomidze, N. K., & Shainidze, J. J. (2021, October). 3D fluorescence spectroscopy of liquid media via internal reference method. In International Conference on Global Research and Education (pp. 59-71). Singapore: Springer Singapore

[62] Khaoua, I., Graciani, G., Kim, A., & Amblard, F. (2021). Detectivity optimization to measure ultraweak light fluxes using an EM-CCD as binary photon counter array. Scientific Reports, 11(1), 3530.

[63] Kodama, S., Kurosawa, S., Ohno, M., Morishita, Y., Usami, H., Hayashi, M., ... & Torii, T. (2020). Fiber-read radiation monitoring system using an optical fiber and red-emitting scintillator for ultra-high-dose conditions. Applied Physics Express, 13(4), 047002.

[64] Konnik, M., & Welsh, J. (2014). High-level numerical simulations of noise in CCD and CMOS photosensors: review and tutorial. arXiv preprint arXiv:1412.4031.

[65] Kundu, S., Roy, P. P., Fleming, G. R., & Makri, N. (2022). Franck–Condon and Herzberg–Teller signatures in molecular absorption and emission spectra. The Journal of Physical Chemistry B, 126(15), 2899-2911.

[66] Lapi, A. J., Blanco, C. R. C., Chierchie, F., Moroni, G. F., Paolini, E. E., Estrada, J., & Tiffenberg, J. (2023). A digital CCD noise reduction technique experimentally tested on a large batch of scientific sensors. IEEE Transactions on Instrumentation and Measurement.

[67] Lapi, A. J., Chierchie, F., Moroni, G. F., Stefanazzi, L., Paolini, E., Estrada, J., ... & Tiffenberg, J. (2022, August). Fast readout of the Skipper CCD for astronomy and quantum imaging. In X-Ray, Optical, and Infrared Detectors for Astronomy X (Vol. 12191, pp. 280-293). SPIE.

[68] Lenhardt Acković, L., Zeković, I., Dramićanin, T., Bro, R., & Dramićanin, M. D. (2018). Modeling food fluorescence with PARAFAC. Reviews in Fluorescence 2017, 161-197.

[69] Li, L., Dai, C., Wu, Z., & Wang, Y. (2017, October). Stray light and bandwidth corrections for commercial CCD array spectrometers. In AOPC 2017: Space Optics and Earth Imaging and Space Navigation (Vol. 10463, pp. 362-368). SPIE.

[70] Luo, Y., Fu, L., & Nan, J. (2023, April). Design of CCD system for deep space spectral imaging detection. In Ninth Symposium on Novel Photoelectronic Detection Technology and Applications (Vol. 12617, pp. 426-434). SPIE.

[71] Maciulevičius, M., Jurkonis, R., Jakovels, D., Raišutis, R., & Tamošiūnas, M. (2024). The evaluation of microbubble concentration using the techniques of optical spectroscopy. Measurement, 114372.

[72] Magdas D. A., Cinta˘ Pinzaru, S., Guyon, F., Feher, I. & Cozar, B. I. Application of SERS technique in white wine discrimination. Food Control. 92, 30–36 (2018).

[73] Maione, B., Brickson, L., Kudenov, M., & Escuti, M. (2016, May). Narrowband emission line imaging spectrometry using Savart plates. In Polarization: Measurement, Analysis, and Remote Sensing XII (Vol. 9853, pp. 68-78). SPIE.

[74] Maniya, N. H., & Srivastava, D. N. (2020). Fabrication of porous silicon based label-free optical biosensor for heat shock protein 70 detection. Materials Science in Semiconductor Processing, 115, 105126.

[75] Mein, P., Malherbe, J. M., Sayède, F., Rudawy, P., Phillips, K. J. H., & Keenan, F. P. (2021). Four decades of advances from MSDP to S4I and SLED imaging spectrometers. Solar Physics, 296, 1-23.

[76] Miller, E. D., Bautz, M. W., Grant, C. E., Foster, R., LaMarr, B., Malonis, A., ... & Reynolds, C. (2023, September). The high-speed X-ray camera on AXIS. In UV, X-Ray, and Gamma-Ray Space Instrumentation for Astronomy XXIII (Vol. 12678, pp. 317-333). SPIE.

[77] Minkova, S., Vladev, V., Hristova-Aqakumova, N., Gabrova, R., Nikolova, K., Evtimov, T., & Hadjimitova, V. (2019, January). Comparative study of the characteristics of red Bulgarian and French wines using applied photonics methods. In 20th International Conference and School on Quantum Electronics: Laser Physics and Applications (Vol. 11047, pp. 142-147). SPIE.

[78] Morse, P. M. (1929). Diatomic molecules according to the wave mechanics. II. Vibrational levels. *Physical Review*, 34(1), 57-64. https://doi.org/10.1103/PhysRev.34.57

[79] Obana, A., Gohto, Y., Tanito, M., Okazaki, S., Gellermann, W., Bernstein, P. S., & Ohira, A. (2014). Effect of age and other factors on macular pigment optical density

measured with resonance Raman spectroscopy. Graefe's Archive for Clinical and Experimental Ophthalmology, 252, 1221-1228.

[80] Obana, A., Ote, K., Gohto, Y., Yamada, H., Hashimoto, F., Okazaki, S., & Asaoka, R. (2024). Deep learning-based correction of cataract-induced influence on macular pigment optical density measurement by autofluorescence spectroscopy. Plos one, 19(2), e0298132.

[81] Paesani, F., & Voth, G. A. (2009). The properties of water: Insights from quantum simulations. The Journal of Physical Chemistry B, 113(17), 5702-5719.

[82] Parigger, C. G., & Hornkohl, J. O. (2019). Quantum Mechanics of the Diatomic Molecule with Applications. IOP Publishing

[83] Prigozhin, G., Cooper, M., Donlon, K., Leitz, C., LaMarr, B., Malonis, A., ... & Bautz, M. (2022, August). Latest results for a fast low noise CCD readout based on pJFET. In X-Ray, Optical, and Infrared Detectors for Astronomy X (Vol. 12191, pp. 471-478). SPIE.

[84] Quatela, A., Gilmore, A. M., Gall, K. E. S., Sandros, M., Csatorday, K., Siemiarczuk, A., ... & Camenen, L. (2018). A-TEEMTM, a new molecular fingerprinting technique: Simultaneous absorbance-transmission and fluorescence excitation-emission matrix method. Methods and Applications in Fluorescence, 6(2), 027002.

[85] Rafik, A., Lakhdar, F., Zouihri, H., Guedira, T., Acharjee, N., Islam, M. S., ... & Zeroual, A. (2024). Experimental and Theoretical Study of Hybrid Dihydrogen Phosphate System: Insights into Bulk Growth, Chemical Etching, Non-Linear Optical Properties, and Antimicrobial Activity.

[86] Reichert, M., Defienne, H., & Fleischer, J. W. (2018). Optimizing the signal-to-noise ratio of biphoton distribution measurements. Physical Review A, 98(1), 013841.

[87] Reusch, W. "Visible and Ultraviolet Spectroscopy". Retrieved 2014-10-29

[88] Russ, R. (2004-09-01). "How Many? A Dictionary of Units of Measurement". Unc.edu. Archived from the original on 1998-12-03. Retrieved 2010-09-20

[89] Rybkin, V. V. (2017). Franck–Condon theory of quantum mechanochemistry. The Journal of Physical Chemistry A, 121(30), 5758-5762.

[90] Saikia, D., Jadhav, P., Hole, A. R., Krishna, C. M., & Singh, S. P. (2022). Growth kinetics monitoring of gram-negative pathogenic microbes using raman spectroscopy. Applied Spectroscopy, 76(10), 1263-1271.

[91] Sampaio, F. G., Del Lama, L. S., Sato, R., de Oliveira, D. M., Czelusniak, C., de Oliveira, L. N., & de Almeida, A. (2013). Quality assurance of a two-dimensional CCD detector system applied in dosimetry. IEEE Transactions on Nuclear Science, 60(2), 810-816.

[92] Sasinska, A., Bialuschewski, D., Islam, M. M., Singh, T., Deo, M., & Mathur, S. (2017). Experimental and theoretical insights into influence of hydrogen and nitrogen plasma on the water splitting performance of ALD grown TiO2 thin films. The Journal of Physical Chemistry C, 121(29), 15538-15548.

[93] Saunders, J. E., Sanders, C., Chen, H., & Loock, H. P. (2016). Refractive indices of common solvents and solutions at 1550 nm. Applied optics, 55(4), 947-953.

[94] Senesi, G. S., Harmon, R. S., & Hark, R. R. (2021). Field-portable and handheld laser-induced breakdown spectroscopy: Historical review, current status and future prospects. Spectrochimica Acta Part B: Atomic Spectroscopy, 175, 106013.

[95] Šesták, J., Planeta, J., & Kahle, V. (2020). Compact optical detector utilizing light emitting diodes, 50 nL L-shaped silica capillary cell and CCD spectrometer for

simultaneous multi-wavelength monitoring of absorbance and fluorescence in microcolumn liquid chromatography. Analytica chimica acta, 1112, 80-91.

[96] Shainidze J., Gomidze N. Creating Fluorescence Spectra Based On The Franck-Condon Factor, Open Readings 2023, p.271

[97] Shainidze, J. J., & Gomidze, N. K. (2023). OPTIMIZING QE OF CCD BY MODIFYING BLACKCOMET DETECTOR. *Book of Abstracts JAPMED*, *12*, 44-46

[98] Shankar, U., Sethi, S. K., Singh, B. P., Kumar, A., Manik, G., & Bandyopadhyay, A. (2021). Optically transparent and lightweight nanocomposite substrate of poly (methyl methacrylate-co-acrylonitrile)/MWCNT for optoelectronic applications: an experimental and theoretical insight. Journal of Materials Science, 56(30), 17040-17061.

[99] Sikorska, E., Włodarska, K., & Khmelinskii, I. (2020). Application of multidimensional and conventional fluorescence techniques for classification of beverages originating from various berry fruit. Methods and Applications in Fluorescence, 8(1), 015006.

[100] Singh, V. R., Choi, H., Yew, E. Y., Bhattacharya, D., Yuan, L., Sheppard, C. J., ... & So, P. T. (2012). Improving signal-to-noise ratio of structured light microscopy based on photon reassignment. Biomedical optics express, 3(1), 206-214.

[101] Small, T. V., Butler, S. D., & Marciniak, M. A. (2021). Uncertainty analysis for CCD-augmented CASI® BRDF measurement system. Optical Engineering, 60(11), 114101-114101.

[102] Smith, C. S., Slotman, J. A., Schermelleh, L., Chakrova, N., Hari, S., Vos, Y., ... & Stallinga, S. (2021). Structured illumination microscopy with noise-controlled image reconstructions. Nature methods, 18(7), 821-828.

[103] Smith, D. R., & Hobson, P. R. (2017). Spectrometer Testing: Dark frame evaluation of StellarNet Black Comet spectrometer.

[104] Spivak, G. (2010). The Comet-FISH assay for the analysis of DNA damage and repair. Fluorescence in situ Hybridization (FISH) Protocols and Applications, 129-145.

[105] Štádlerová, B., Dědina, J., & Musil, S. (2023). Comparison of bismuth atomic lamps for a non-dispersive atomic fluorescence spectrometry. Spectrochimica Acta Part B: Atomic Spectroscopy, 205, 106692.

[106] Štádlerová, B., Kolrosová, M., Dědina, J., & Musil, S. (2020). Atomic fluorescence spectrometry for ultrasensitive determination of bismuth based on hydride generation–the role of excitation source, interference filter and flame atomizers. Journal of Analytical Atomic Spectrometry, 35(5), 993-1002.

[107] Stroyuk, O., Raievska, O., Osvet, A., Hauch, J., & Brabec, C. J. (2023). An insight into the temperature dependence of photoluminescence of a highly-emissive Cs-Ag (Na) Bi (In) Cl 6 perovskite. Journal of Materials Chemistry C, 11(13), 4328-4332.

[108] Suciu, R. C., Zarbo, L., Guyon, F., & Magdas, D. A. (2019). Application of fluorescence spectroscopy using classical right angle technique in white wines classification. Scientific reports, 9(1), 18250.

[109] Sugiura, Y., & Takayanagi, T. (2020). Franck–Condon simulations of transition-state spectra for the OH+ H 2 O and OD+ D 2 O reactions. Physical Chemistry Chemical Physics, 22(36), 20685-20692.

[110] Sun, X., Wang, X., Wang, F., Cao, Y., Ding, X., Dou, Y., ... & Huang, C. (2024). Reconstruction Filters Improving the Spatial Resolution and Signal-to-Noise Ratio of Surface Plasmon Resonance Microscopy. Analytical Chemistry, 96(2), 636-641.
[111] Tadgell, B., Ponomareva, E., Karg, M., & Mulvaney, P. (2022). Temperature-Jump Spectroscopy of Gold–Poly (N-isopropylacrylamide) Core–Shell Microgels. The Journal of Physical Chemistry C, 126(8), 4118-4131.
[112] Videen G., Ngo D. "Light Scattering from a Cell," in Optics of Biological Particles, NATO Science Series, Series II: Mathematics, Physics and Chemistry, Vol. 238, (A. Hoekstra, V. Maltsev, and G. Videen, eds.), New York: Springer, 2007.
[113] Villalpando, E. M., Drlica-Wagner, A., Malagón, A. A. P., Bakshi, A., Bonati, M., Campa, J., ... & Tiffenberg, J. (2023). Characterization and Optimization of Skipper CCDs for the SOAR Integral Field Spectrograph. arXiv preprint arXiv:2311.00813.
[114] Wang, A., Xing, S., Zhao, Y., Wu, H., & Iwahori, Y. (2022). A hyperspectral image classification method based on adaptive spectral spatial kernel combined with improved vision transformer. Remote Sensing, 14(15), 3705.
[115] Wang, L. V., & Wu, H. I. (2007). Biomedical optics: principles and imaging. John Wiley & Sons
[116] Wilhelm, P., Vogelsang, J., Schönfelder, N., Höger, S., & Lupton, J. M. (2019). Anomalous linear dichroism in bent chromophores of π-conjugated polymers: departure from the franck-condon principle. Physical Review Letters, 122(5), 057402.
[117] Zacharioudaki, D. E., Fitilis, I., & Kotti, M. (2022). Review of fluorescence spectroscopy in environmental quality applications. Molecules, 27(15), 4801
[118] Zhang, D., Wang, R., Wang, X., & Gogotsi, Y. (2023). In situ monitoring redox processes in energy storage using UV–Vis spectroscopy. Nature Energy, 8(6), 567-576.
[119] Zhang, L., Li, B., Li, H., Gu, G., & Wang, X. (2023). Signal-to-noise ratio analysis based on different space remote sensing instruments. IEEE Photonics Journal.
[120] Zhang, Y., Wang, H., Li, H., Sun, J., Liu, H., & Yin, Y. (2022). Optimization model of signal-to-noise ratio for a typical polarization multispectral imaging remote sensor. Sensors, 22(17), 6624.
[121] Zixuan Fu , Xianfeng Zheng , Jun Liang, A general analytical expression for evaluation of an arbitrary n-dimensional Franck-Condon overlap integral including the Duschinsky effect, Computational and Theoretical Chemistry 1207 (2022) 113501